Interactions between Hippocampal Areas CA3 and CA1 during Slow-Wave Sleep

Thesis by

Ming Gu

In Partial Fulfillment of the Requirements

for the Degree of

Doctor of Philosophy

California Institute of Technology

Pasadena, California

2010

(Defended December 4, 2009)

For Mom, Dad, Jane, and Ethan.

Acknowledgments

First, I would like to thank my advisor, Thanos Siapas, who for the past six years has given me exceedingly generous support and perpetual commitment of his time, effort, and patience. I would also like to thank the rest of my thesis committee, Michael Elowitz, Gilles Laurent, and Erin Schuman, for all their helpful suggestions and insightful comments to my work, and their friendliness and encouragement during the past six years. I am also immensively grateful to my labmates: Eugene Lubenov, who is my major collaborator on this project, and Andreas Hoenselaar and Casimir Wierzynski, who have contributed tremendous time and effort in giving me thoughtful suggestions and scientific feedbacks for this work. Both Cas and Eugene also generously provided me with some of their own data for this work. Last, but not the least, nothing is possible without the dedication and technical wizardry from Mike Walsh.

This work was supported by the Norris Foundation, the Liming Foundation, the Caltech Information Science and Technology Center for Biological Circuits Design, the James S. McDonnell Foundation, the Bren Foundation, the McKnight Foundation, the Whitehall Foundation, and the National Institutes of Health.

Abstract

Many lines of evidence suggest that the hippocampus plays a critical role in memory formation. The predominant hypothesis is that new memories are initially stored within hippocampal circuits during awake behavior, and are subsequently consolidated across neocortical networks under the influence of hippocampal activity during sleep. The hippocampal memory trace is conjectured to reside within the recurrent circuits of area CA3, which is believed to function as an autoassociative memory. Area CA3 projects almost exclusively to area CA1, one of the major output stages of the hippocampus. How is CA3 activity transformed in CA1, and what is the function of the CA1 subfield that intermediates between CA3 and the neocortex, the presumed long-term storage site of memories?

Here we characterize the relationships between CA3 and CA1 activity during slow-wave sleep (SWS), a stage of sleep conjectured to be important in memory consolidation. Activity in SWS is marked by the presence of short-lived ($\sim$100 ms) population bursts that are believed to be spontaneously generated within CA3 and that co-occur with high-frequency oscillations ($\sim$200 Hz ripples) in area CA1. We demonstrate that:

1. CA1 amplifies transient increases in CA3 activity levels, while attenuating background fluctuations.

2. The fraction of co-active neurons is higher in CA1 than in CA3, while the firing intensity of active neurons is higher in CA3 than in CA1.

3. The above dichotomy is particularly pronounced during the population bursts associated with ripples.

4. In comparison to isolated spikes, bursts of action potentials by CA3 neurons

are particularly effective at triggering large CA1 responses and predicting the onset of CA1 ripples.

These results show that CA1 acts as a selective filter and amplifier of CA3 activity patterns, and that bursting of individual CA3 neurons plays a special role in this CA3-CA1 transformation. We hypothesize that coordinated bursts in CA3 reflect convergence to attractors, each representing a stored pattern in the auto-associative network. Our observations suggest that these stored patterns are preferentially amplified by CA1 and transmitted to downstream targets, while activity representing intermediate states in-between attractors are less likely to be transmitted.

Contents

List of Figures

List of Tables

Chapter 1

Introduction

1.1 Hippocampal Role in Memory Formation

Many lines of evidence suggest that the hippocampus plays a critical role in forming new memories, but is not the long-term storage site for these memories[1,2]. In humans, bilateral hippocampal lesions leave patients unable to form new memories while sparing remote memories, a condition called anterograde amnesia[3]. In rats, hippocampal lesions impair a wide variety of memory tasks, which include navigating the Morris water maze[4], odor-discrimination learning[5], and spatial alternation[6]. Furthermore, for certain associative learning tasks such as trace eyeblink conditioning, learning impairment due to hippocampal lesion is also time-dependent. As the interval between learning and hippocampal lesion increases, the effect of the lesion on acquired memory diminishes[7].

According to one widely held model, memories are formed in two stages[8]. In the first stage, during wakefulness, sensory stimuli reach the hippocampus through neocortex and initial memory traces are embedded within hippocampal circuits (Fig. 1.1, left). In the second stage, during sleep, spontaneous hippocampal activity independent of any sensory stimuli triggers synaptic changes both within the hippocampus and across cortical circuits. Through this process, the initial memory traces are further reorganized within the hippocampus and gradually transferred to the neocortex where they are permanently stored and can be recalled independently of the hippocampus

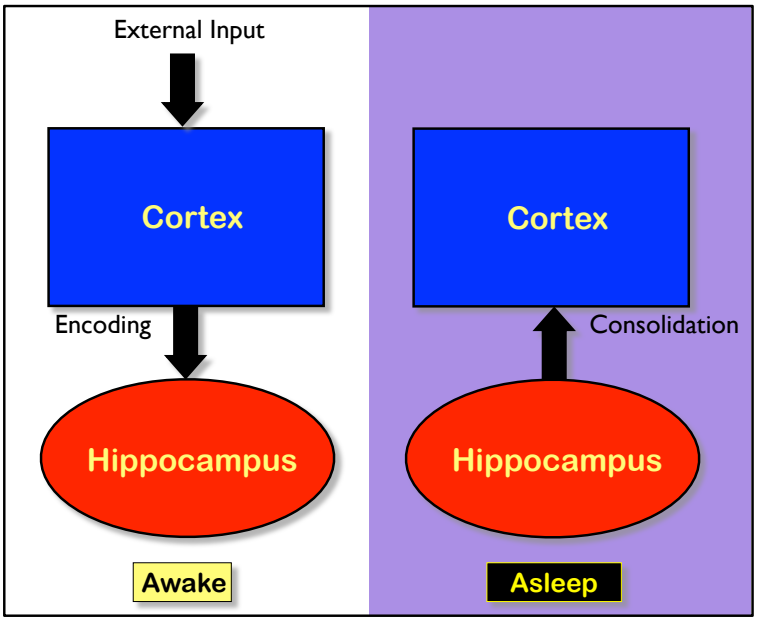

Figure 1.1: **The two-stage model of memory formation.**

(Fig. 1.1, right).

1.2 Role of CA3 in Initial Memory Storage

The hippocampus is a heterogeneous structure with subfields that have very different architectures. The functional roles of the different subfields are not known, although anatomy can provide some insights. In particular, the hippocampus consists of four subfields: the dentate gyrus, area CA3, area CA1, and the subiculum (Fig. 1.2). These subfields are defined based on their distinct cell morphologies and connectivity patterns.[9]. Furthermore, unlike many other brain structures where the coexistence of both feed-forward and feedback connections is the norm, major intrinsic connections within the hippocampus can be characterized by a mostly feed-forward trisynaptic pathway: the perforant pathway from entorhinal cortex to dentate gyrus, mossy fibers from dentate gyrus to area CA3, and Schaffer collaterals from area CA3 to area CA1 (Fig. 1.2).

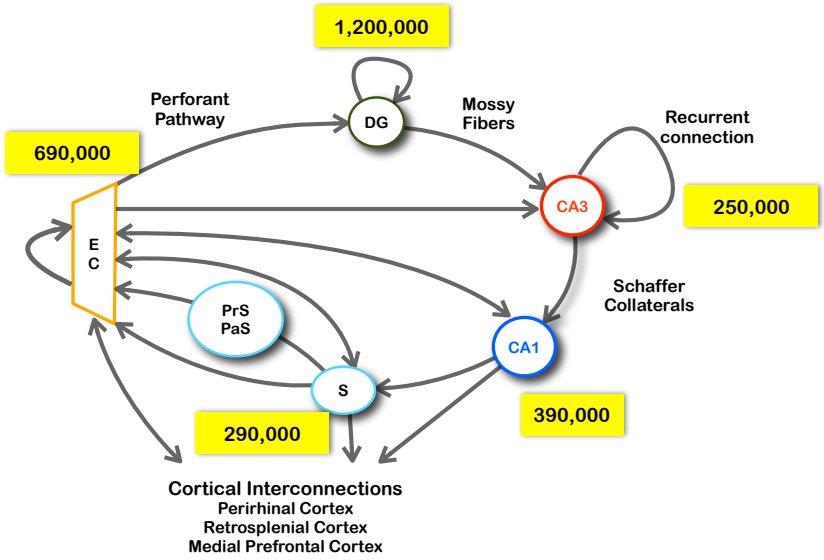

Figure 1.2: **Subfields and connections of the rat hippocampus.** Numbers in yellow rectangles indicate pyramidal cell counts in each hippocampal subfield per hemisphere. Projections are shown as arrows. Note the trisynaptic pathway that originates from entorhinal cortex and ends at area CA1. EC, entorhinal cortex. DG, dentate gyrus. S, subiculum. Prs, presubiculum. PaS, parasubiculum. Adapted from[9]. Cell counts from[10].

Among hippocampal subfields, area CA3 represents the most likely storage site for initial memory traces. Theoretical work in artificial neural networks has shown that recurrent circuits with Hebbian synapses can function as an autoassociative memory[11]. Highly extensive recurrent connections exist within CA3[9]. The arborized axon of a CA3 pyramidal cell can make dendritic contacts to several thousands of other CA3 neurons[12]. Furthermore, CA3-CA3 synapses are highly plastic and display a Hebbian form of activity-dependent synaptic modification[13]. Therefore, these unique anatomical and physiological features provide a foundation for CA3 to operate as an autoassociative memory network[14,15,16]. Many theoretical and experimental studies have suggested that CA3 may encode and store recent memories temporarily in its recurrent circuits before facilitating their permanent transfer to the neocortex[17,18,19,20,21]. This is consistent with the two-stage model of memory formation (Fig. 1.1), whereby the initial encoding phase occurs during the awake state and the transfer phase occurs during sleep. Additional support of CA3's role in both the encoding and the transfer of mem-

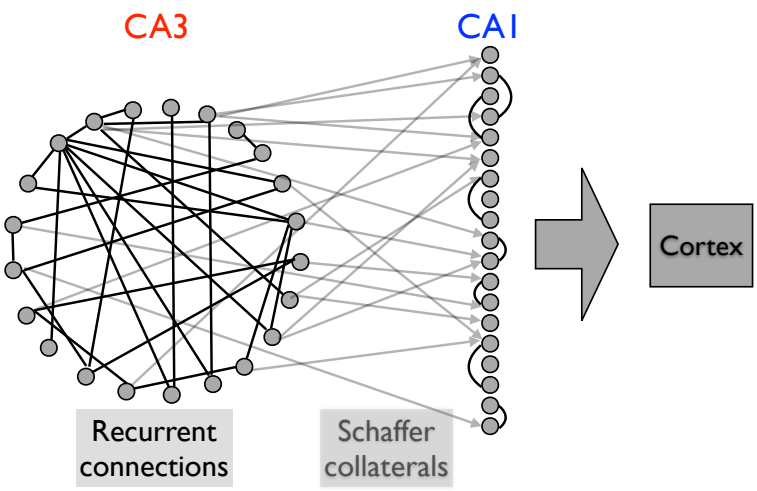

Figure 1.3: **Anatomical differences between are CA1 and CA3.** In rats, both CA1 and CA3 have approximately 200,000 to 400,000 pyramidal cells per hemisphere. There are dense recurrent connections within CA3, which also projects to CA1 extensively through Schaffer collaterals. CA1 further projects to many cortical regions. A major difference between the two areas is that there are significantly fewer recurrent connections in CA1 compared to CA3.

ories has come from recent genetic manipulations of CA3 in rodent models. NMDA receptor deletion restricted to CA3 impairs the rapid encoding of novel information[22], while posttraining blockade of CA3 output impairs the consolidation of contextual fear memory[23].

1.3 Role of CA1 in Memory Formation

If CA3 acts as the temporary storage site for recent memories before their transfer to the neocortex, then the role of area CA1 becomes puzzling. With the exception of a few subcortical nuclei[24,25], CA3 projects almost exclusively to CA1 through Schaffer collaterals[26,27]. This projection is extensive, with each CA3 pyramidal cell giving rise to arborized axonal plexuses that fan out to as much as 75% of the septotemporal extent of CA1[12]. Moreover, among hippocampal subfields, CA1 has the highest degree of cytoarchitectonic similarity to CA3: both areas have similar laminar structures, overlapping cell types, and contain roughly the same number of pyramidal

cells[9] (Fig. 1.2). However, one feature that clearly differentiates the two areas is the presence of highly extensive recurrent connections within CA3 compared to the paucity of such connections within CA1[28] (Fig. 1.3). Futhermore, unlike CA3, CA1 projects either directly or through the subiculum and entorhinal cortex to a wide range of cortical areas downstream from the hippocampus[29,30,31,32].

What is the role of CA1, which is anatomically positioned as the sole bridge of communication between CA3, the putative temporary storage site for recent memories, and the neocortex, the permanent storage site for long-term memories? In order to understand the process of memory formation, therefore it is crucial to study how CA3 neuronal activity is transformed by CA1 on its way to the neocortex. This will be the focus of this thesis.

1.4 CA3-CA1 Transformation in Slow-Wave Sleep

We concentrate on slow-wave sleep (SWS) in our study of CA3-CA1 transformation for the following reasons. First, it has been hypothesized that recent memory is transferred from hippocampus to neocortex during sleep (stage 2 of the two-stage model of memory formation, Fig. 1.1, right). Second, SWS provides a unique opportunity for probing the CA3-CA1 circuit independent of external input. During SWS, external input from the entorhinal cortex to hippocampus is highly attenuated[33,34], and spontaneous CA3 activity is thought to provide the dominant drive for the CA3-CA1 circuit[35]. In contrast, the entorhinal cortex is believed to strongly influence both CA3 and CA1 activity during awake behavior. Furthermore, hippocampal activity during SWS is characterized by the presence of *ripples*. Ripples are characterized by large high-frequency (80 – 400 Hz) oscillations in CA1 local field potentials (LFPs) and increased firing in the entire hippocampus within a short ($\sim$100 ms) time window[36,37] (Fig. 1.4). Recent evidence has shown that synchronous CA1 firing during ripples may play a crucial role in communication between the hippocampus and the prefrontal cortex[38]. Coordinated CA1 spiking within such a short time interval provides a strong

depolarizing force that may engage plasticity mechanisms in neocortical targets. In addition, coherent discharge of a small group of CA3 neurons is believed to trigger hippocampal ripples[35].

1.5 Outline

The rest of this thesis is organized as follows. First, we characterize the relationship between CA3 and CA1 population firing rates in SWS and demonstrate that on average CA1 effectively amplifies only those fluctuations in CA3 spiking levels that exceed the background rate by a factor of two or more. Next, by analyzing the firing of single pyramidal cells in both areas, we show that during SWS a larger fraction of neurons are co-activated in CA1 compared to CA3, while CA3 neurons discharge more spikes than CA1 when activated. This dichotomy between population burst size and unit burst size is particularly pronounced during ripples. Based on these observations, we hypothesize that CA1 population events are launched by a smaller coordinated set of CA3 neurons firing bursts of spikes. We present several lines of evidence in support of this hypothesis. In particular, CA3 bursts are more effective than single spikes at triggering large CA1 responses and predicting the onset of ripples. Longer CA3 bursts tend to occur progressively earlier with respect to ripple onsets. Overall, our observations argue that during SWS CA1 may act as a selective amplifier of CA3 activity patterns and that bursting of individual CA3 neurons may play a special role in this transformation. Finally, we discuss possible mechanisms that may be responsible for such a transformation and its possible role in memory formation.

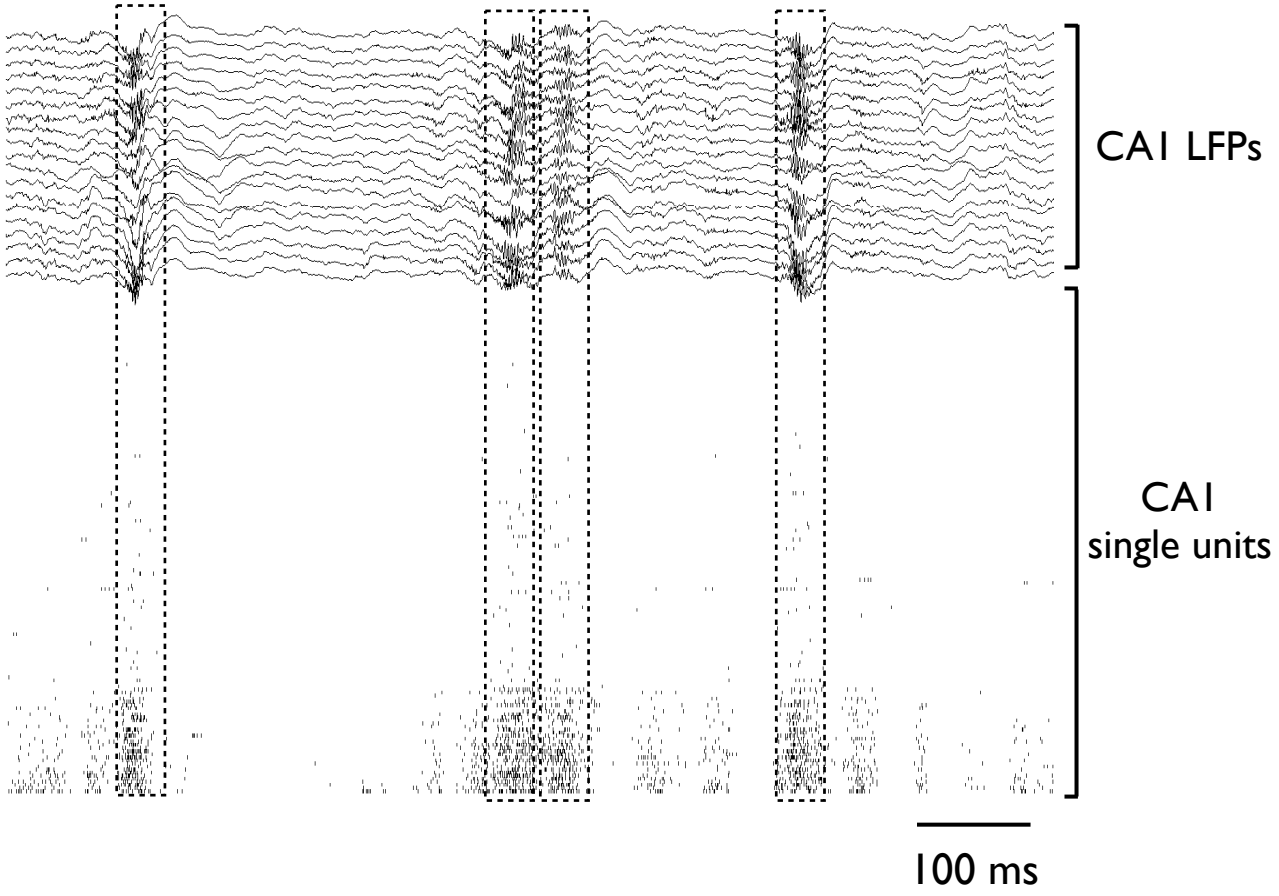

Figure 1.4: **Ripple events in hippocampal CA1 pyramidal layer.** LFP from 19 CA1 tetrodes (1 channel per tetrode) and raster plot of single unit activity from 140 CA1 units, ordered in terms of their firing rate. Ripples are marked by dotted rectangles. Notice the high-frequency oscillations in the LFPs coincide with increased discharge of CA1 neurons. Most pyramidal cells fire no more than a few spikes in a given ripple, while interneurons (the ones close to the bottom of the raster plot) fire more spikes and in more ripples.

Chapter 2

Experimental Results

2.1 CA1 Amplifies CA3 Activity during SWS

Our first objective was to characterize the relationship between CA3 and CA1 activity in slow-wave sleep (SWS). We first focused on population firing rates, computed from the multiunit activity containing all recorded spikes, and the 80 – 400 Hz ripple band of the local field potentials (LFPs). Figure 2.1A shows an example of spiking and LFPs simultaneously recorded in CA1 and CA3. This example illustrates several key features. First, there are brief episodes of sharply increased population firing rate in both CA1 and CA3, with the relative increases in CA1 larger than those in CA3. Second, these episodes coincide with large high-frequency oscillations in CA1 LFPs (ripples). Third, CA1 population firing rate co-varies with CA3 most of the time, especially at higher activity levels. Finally, when CA3 population firing rate is at relatively low levels, CA1 does not necessarily co-vary with CA3 activity. These observations are confirmed in the summary plots in Figure 2.1B: 1) The dynamic range is larger for CA1 population firing rate than for CA3 and CA1 spends more time in higher firing rates (Fig. 2.1B(i)). 2) When the CA3 population firing rate exceeds twice the background level, CA1 amplifies CA3 input (Fig. 2.1B(ii)), 3) and these higher rate episodes coincide with hippocampal ripples (Fig. 2.1B(iii)).

While Figure 2.1A illustrates differences between CA3 and CA1 activity over the span of just a few seconds, our recordings spanned many hours and multiple sleep

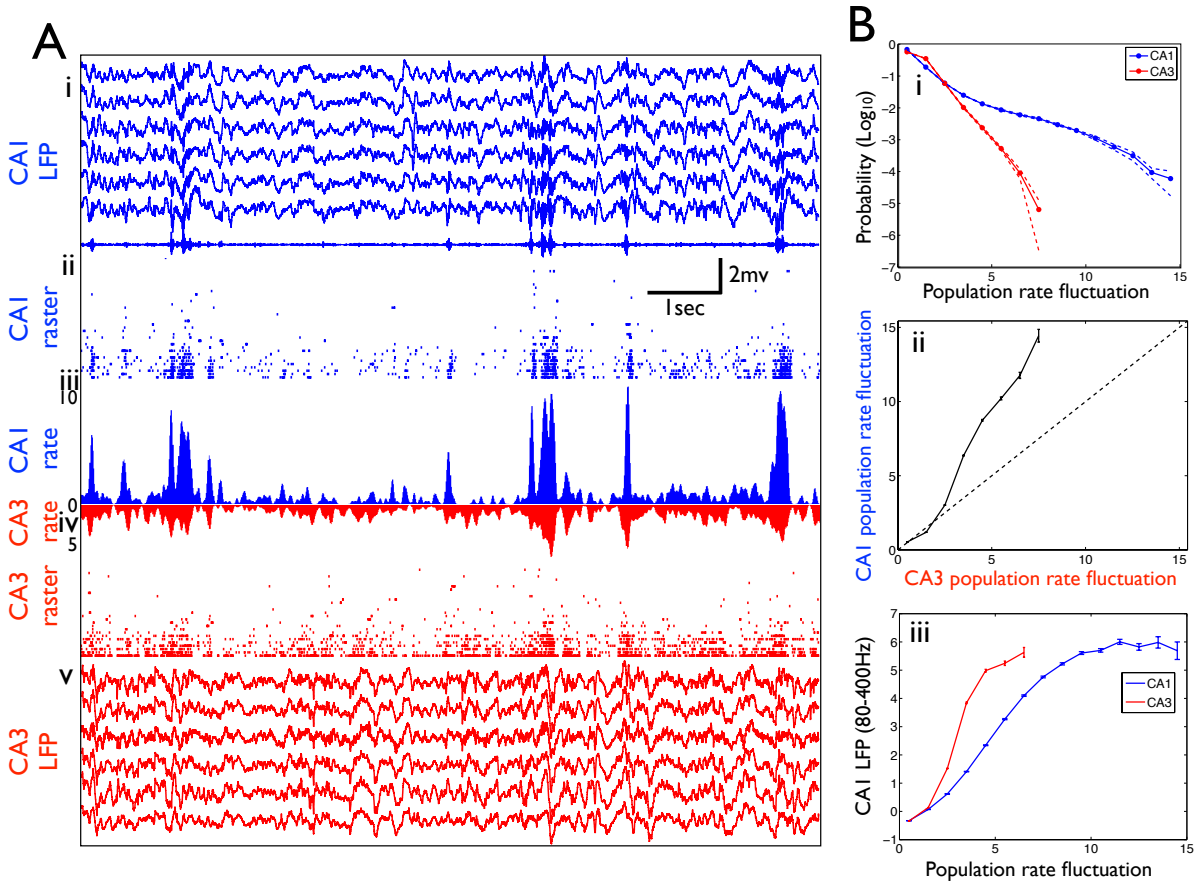

Figure 2.1: **Hippocampal CA1 amplification of CA3 activity during SWS. A: (i,v)** Local field potentials (LFPs) from 6 CA1 tetrodes (in blue) and 6 CA3 tetrodes (in red). One channel per tetrode is plotted. The LFP trace from the last CA1 tetrode is filtered in 80 – 400 Hz band and is plotted as the bottom trace. **(ii,iv)** Rasters of 39 CA1 units and 46 CA3 units, ordered by firing rate. **(iii)** Population firing rate fluctuations in CA1 and CA3: all recorded spikes are histogramed into 10 ms bins, smoothed with a 100 ms Gaussian window, and the resulting population firing rate is divided by its time average. The resulting dimensionless quantity measures the fluctuations in activity levels relative to the background level. Note that high-frequency oscillation in CA1 LFP coincides with increased activity in both CA1 and CA3. **B: (i)** Distributions of population firing rate fluctuations in CA3 (in red) and CA1 (in blue). Dashed lines indicate standard errors across 10 SWS epochs. Note that fluctuations in CA1 are larger than those in CA3. **(ii)** Average relationship between CA3 and CA1 firing rate fluctuations. Note that once activity in CA3 is at least twice above the background level, the corresponding activity in CA1 is significantly amplified (black curve is above the diagonal). **(iii)** The relationship between CA1 (in blue) and CA3 (in red) population firing rate fluctuations and CA1 LFP amplitude in the ripple band. LFP amplitude is calculated from the amplitude measurements of the Hilbert transform of the LFP traces filtered in 80 – 400 Hz. The resulting values are then transformed into Z-scores. Note that high population firing rate in both areas coincides with large high-frequency oscillations in CA1 LFPs.

stage transitions between SWS, REM, and AWAKE. For example, Figure 2.2A tracks the interactions between the two areas over more than 9 hours. Our analysis shows that the strongest CA3-CA1 interactions are restricted to SWS (Fig. 2.2A(ii)) and that CA3 firing tends to precede CA1 activity by several milliseconds (Fig. 2.2B), consistent with the view that population bursts and ripples in CA1 are triggered by firing in CA3[35].

2.2 Area Differences in Population and Single-Unit Bursting during SWS

Population firing rate is determined by both the number of co-active neurons in a given time interval and the number of spikes each active neuron produces in that same interval. Going beyond the multiunit level, we next investigated how CA1 and CA3 behave along these two dimensions during SWS at the single-cell level. We restricted our analysis to putative pyramidal cells (428 CA1, 190 CA3 cells), which were identified as those units with average firing rate below 1 Hz over the duration of the recording session.

We defined *population burst size* over a given time interval as the fraction of simultaneously recorded neurons that fire at least 1 spike during that interval. We used a 100 ms window in this study, because it is close to the mean ripple duration. The main observations to be presented here are not affected by the choice of any time interval between 20 and 500 ms. According to this measurement, we discovered that CA1 tends to exhibit higher population burst sizes than CA3 during SWS (Fig. 2.3B). When 50 neurons per dataset were used to compute population burst size, we found the average population burst size to be 0.86% for CA3 (n = 326,289, 9.1 hr total over 2 datasets; s.e. = 0.003%) and 1.48% for CA1 (n = 175,835, 4.9 hr total over 4 datasets; s.e. = 0.007%). Furthermore, this difference is independent of the number of neurons used in computing the population burst size (Fig. 2.4A), although a larger

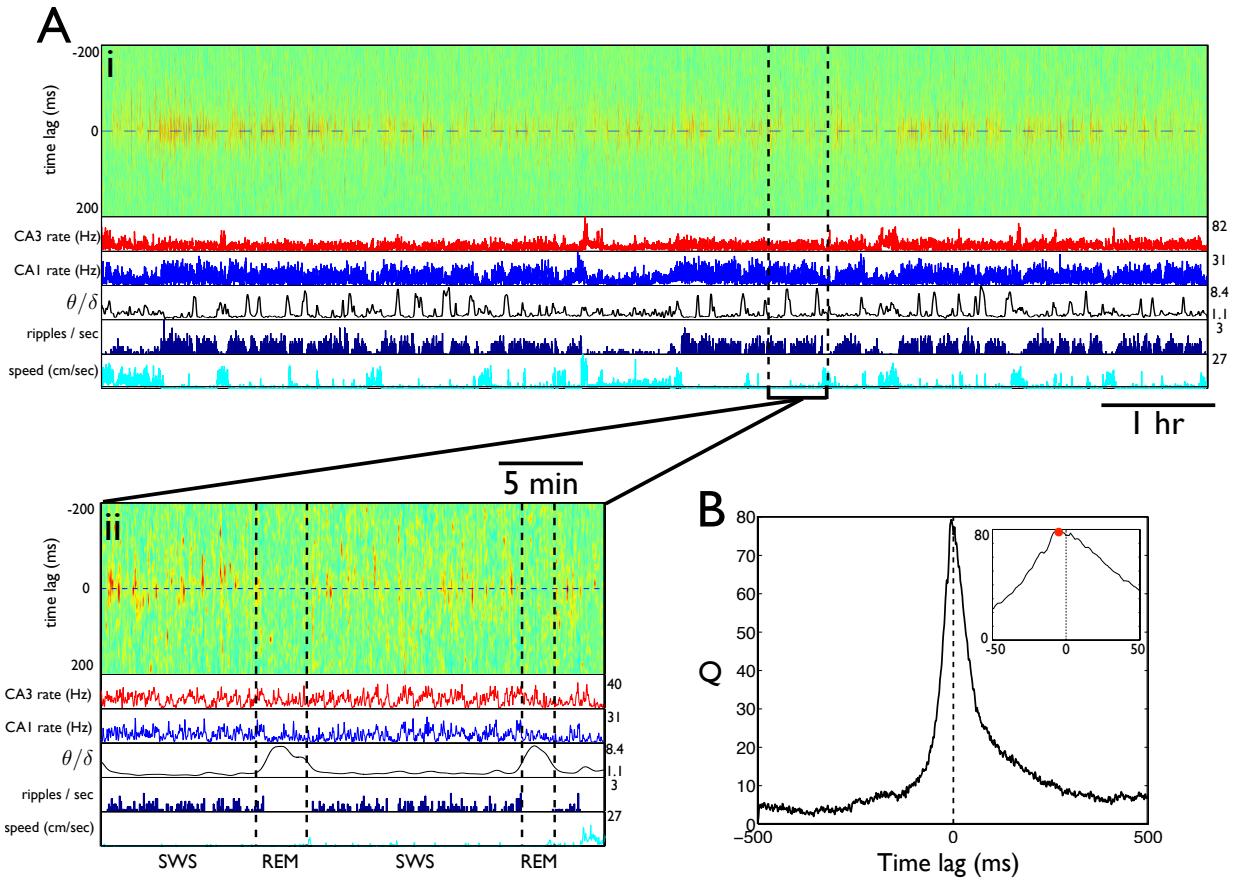

Figure 2.2: **CA1 and CA3 activity during sleep. A: (i)** X-axis: time. From top to bottom, the panels show: Each vertical line represents standardized cross-covariance over rolling 5 sec windows between CA3 and CA1 multiunit activity (the top color panel, see Chapter 4 for details of standardized cross-covariance); CA3 (in red) and CA1 (in blue) multiunit firing rate in 1 sec bins smoothed over 5 bins; ratio of theta to delta amplitudes in the LFP (in black, see Chapter 4 and [38] for how this is computed); ripple density in 5 sec bins (in blue); speed of the animal (in cyan). Position is sampled at 30 Hz and smoothed over 5 seconds. Note that SWS, REM, AWAKE can be segmented using a combination of theta to delta ratio (high in AWAKE and REM, low in SWS), ripple density (high in SWS, low in REM) and animal speed (high in AWAKE, low in SWS and REM) (see [38] for details of sleep stage segmentation). **(ii)** A 30 minute segment of (i). Note that episodes of higher cross-covariance between CA3 and CA1, shown as hot colors in the top panel, are short in duration and are almost restricted to SWS. **B:** Standardized cross-covariance between CA3 and CA1 multiunit activity during SWS. Maximum lag = 500 ms. Bin size = 1 ms, smoothed by 3 bins. Inset: zoom at $\pm$50 ms window. Note the peak (red dot) at -6 ms, indicating that on average CA3 spiking precedes CA1 spiking.

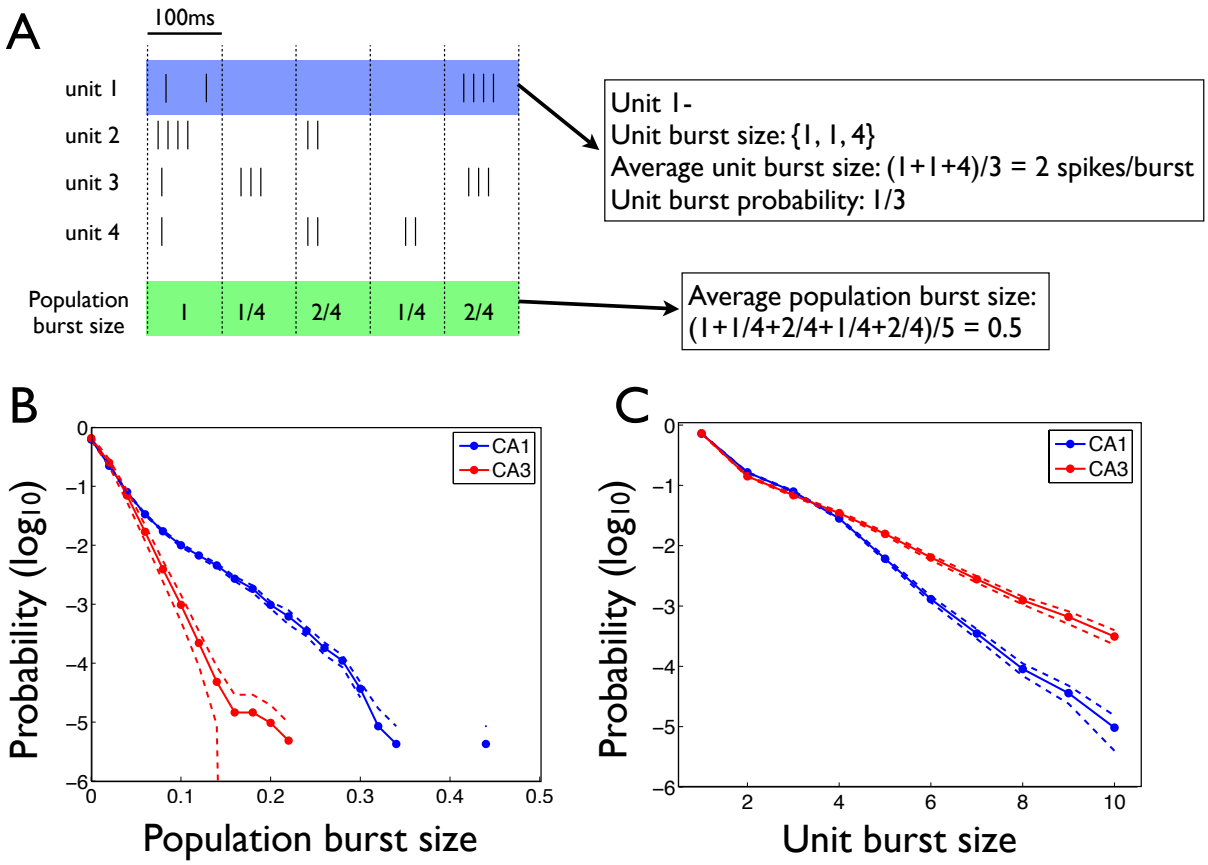

Figure 2.3: **Population burst size and unit burst size in SWS. A:** Illustration of how population burst size and unit burst size are calculated. **B:** Distributions of population burst sizes, expressed as a fraction of the simultaneously recorded neurons. Dashed lines indicate standard errors. To avoid complications due to difference in number of neurons recorded across datasets, 50 cells in an area are randomly sampled from each dataset that contains at least 50 cells in that area. Note that a larger proportion of neurons in CA1 are active than in CA3. CA1: n = 4 datasets. Average population burst size = 1.5%; CA3: n = 2 datasets. Average population burst size = 0.9%. **C:** Distributions of unit burst sizes. For each neuron, spikes occurring within 20 ms from each other are grouped into bursts and the size of each burst is given by the number of spikes it contains. Thus bursts of size 1 correspond to isolated spikes, bursts of size 2 contain two spikes, etc. Note that CA3 neurons are more likely to fire longer bursts than CA1 neurons. CA1: n = 420 cells. CA3: n = 189 cells.

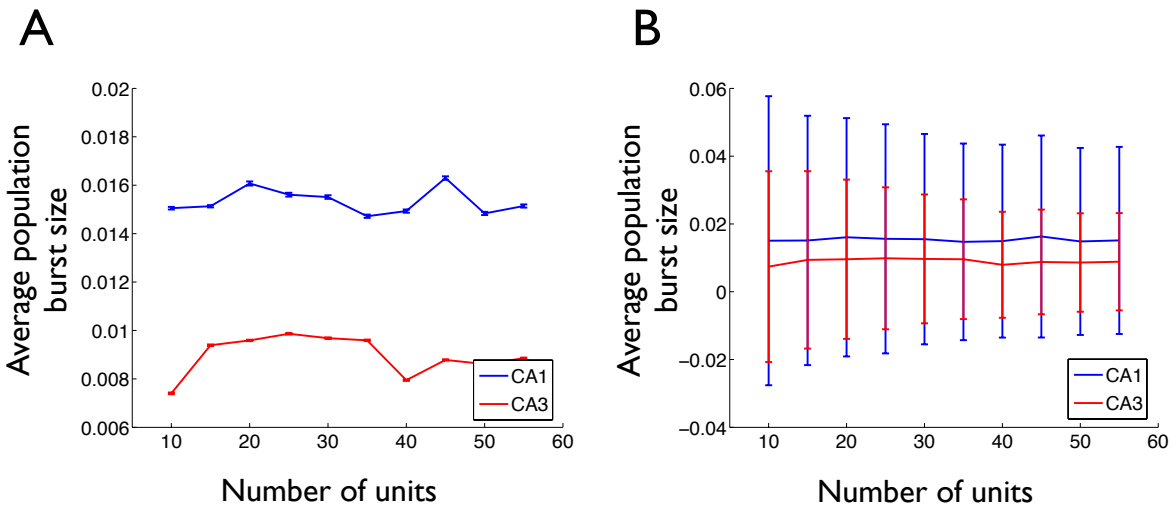

Figure 2.4: **Average population burst size during SWS computed using different number of neurons. A:** Average population burst size as a function of the number of units used to compute it. Note that population burst size fluctuates with the number of units used, but the difference between CA3 and CA1 remains significant. Standard errors are shown. Note due to the large sample number, error bars are barely visible in the plot. **B:** Same plot as **A**, but standard deviations, instead of standard errors, are plotted here. Note that as the number of units increases, the standard deviation of resulting population burst sizes decreases.

number decreases the standard deviation of its distribution (Fig. 2.4B). Additionally, in line with the difference in population burst sizes between the two areas, more pairs of pyramidal cells in area CA1 are correlated than in area CA3 (Fig. 2.5).

We next focused on the other dimension: the number of spikes a neuron fires when activated. Pyramidal cells in the hippocampus tend to fire a series of action potentials (APs) with short interspike intervals (ISIs). These events are called *complex spikes* or *bursts*[39,40]. In this study, we defined a *unit burst* as a sequence of any number of consecutive spikes with ISI $\leq$ 20 ms (see Chapter 4 and Fig. 4.2 for how this threshold was chosen). We also defined *unit burst size* as the number of spikes in a burst. A burst of size one is an isolated single spike. Using this measurement, we observed that CA3 pyramidal cells tend to fire longer bursts, with some as long as 20 spikes, while the distribution of unit burst sizes for CA1 neurons is more skewed toward shorter (2-3 spike) bursts (Fig. 2.3C, Fig. 2.6). However, it should also be noted that as reported *in vitro*[41,42], the tendency to fire multiple spikes in a burst is not homogeneous across

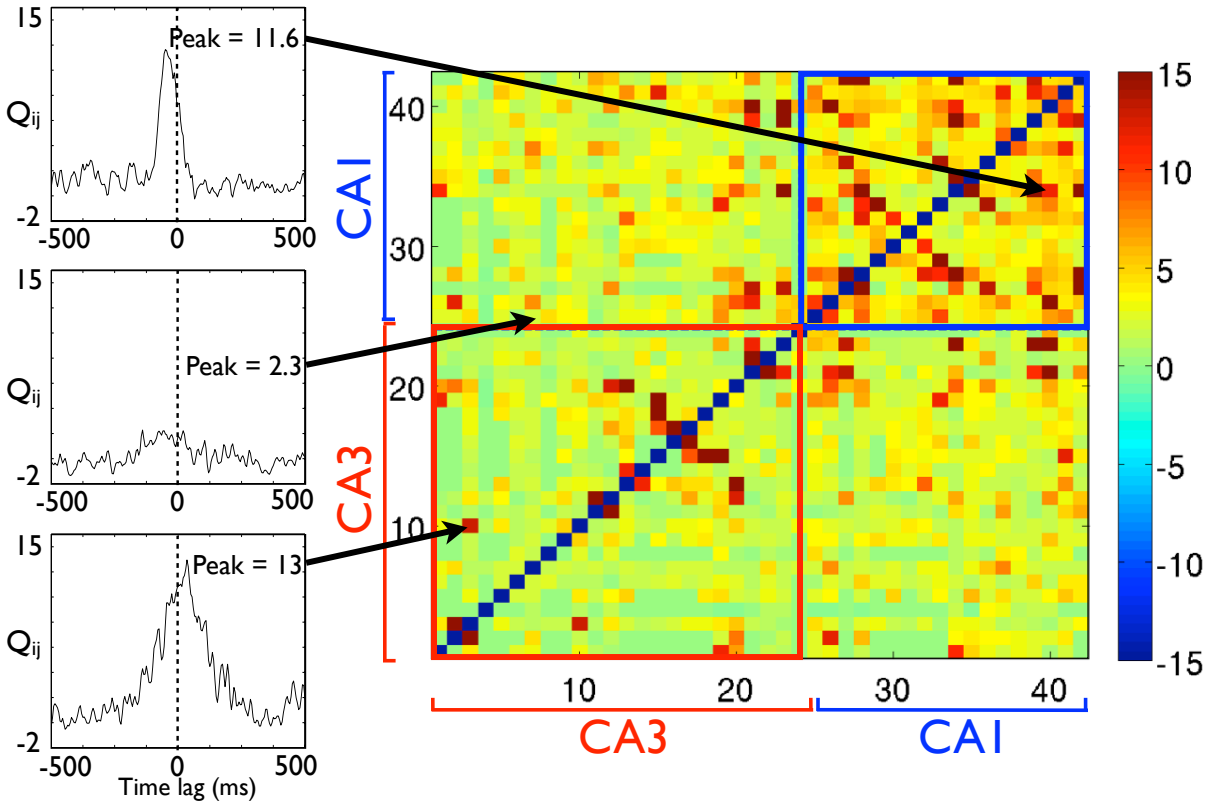

Figure 2.5: **Peak standardized cross-covariance matrix.** Left: three examples of standardized cross-covariances between pairs of neurons within CA1 (top), across CA3 and CA1 (middle), and within CA3 (bottom). See Chapter 4 for how standardized cross-covariance is computed. Right: Each box pixel represents the peak standardized cross-covariance between spikes from a pair of neurons. Bin size = 2 ms. Maximum lag = 200 ms. Note there are more pairs of neurons in CA1 with high cross-covariance than in CA3.

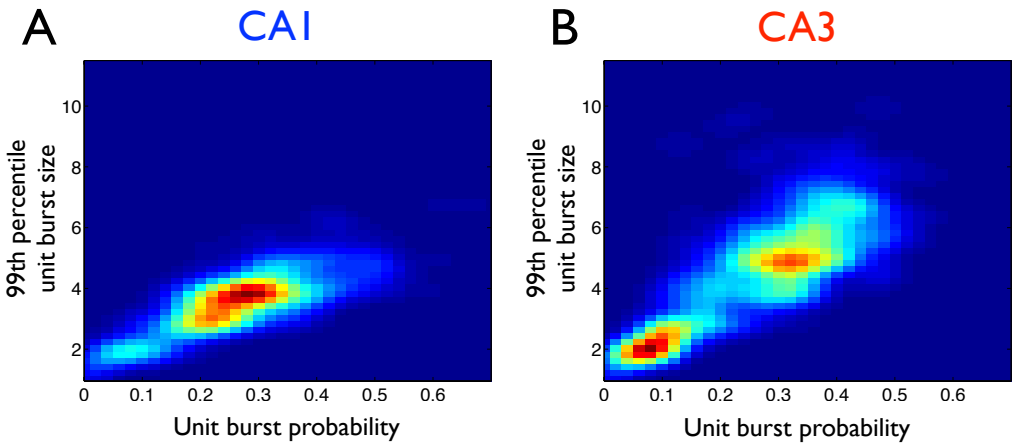

Figure 2.6: **Unit burst probability and 99th percentile unit burst size of CA1 and CA3 neurons.** 2D histogram of unit burst probability and 99th percentile unit burst size for CA1 (A) and CA3 neurons (B) during SWS. Unit burst probability is calculated as the percentage of bursts of size ≥ 2 (see Fig. 2.3A). 99th percentile unit burst size is the minimal burst size of the top 1% of bursts ordered by size. Note that there are a group of neurons that tend not to fire multiple-spike bursts in both areas. Also note that among the bursting cells, CA3 neurons tend to fire multiple-spike bursts more often and have larger unit burst sizes than CA1 neurons. CA1: n = 420 cells. CA3: n = 189 cells.

all neurons in the hippocampus. As is shown in Fig. 2.6, in both CA1 and CA3, there are a collection of neurons that rarely fire multiple-spike bursts (also see Fig. 4.1 and Fig. 4.3).

2.3 Ripples Accentuate Area Differences in Bursting

Since firing in CA3 is believed to trigger ripples in CA1 and ripples may play a crucial role in memory formation (see Chapter 1), it is important to characterize how these differences in population burst size and unit burst size between CA1 and CA3 change during ripples. Any dependence of these differences on the macroscopic state of the hippocampal network[40] — i.e., ripple versus non-ripple — would constrain theories of how CA3 activity is transformed by CA1. Thus, we next compared CA1 and CA3 activity along the two dimensions, population burst size and unit burst size, both inside and outside ripples.

To make this comparison, we first identified ripple events by detecting epochs of

high CA1 LFP power in the 80 – 400 Hz band (see methods described in Chapter 4 for details). We then partitioned SWS into two subsets: ripple epochs, consisting of 100 ms windows centered around each ripple, and non-ripple epochs, which contained everything else. We then computed population burst size and unit burst size in these two subsets. Not surprisingly, we found that population burst size is higher inside compared to outside ripples for both CA1 and CA3 (Fig. 2.7A). However, while this increase is $\sim$3 fold for CA3, it is $\sim$8 fold for CA1. As is shown in Fig. 2.7A(ii), compared to 0.8% CA3 (n = 312,863, 8.7 hr over 2 datasets; s.e. = 0.003%) and 1.1% CA1 (n = 166,420, 4.6 hr over 4 datasets; s.e. = 0.005%) pyramidal cells being active in a 100 ms window outside ripples, 2.3% CA3 (n = 13,526 ripples over 2 datasets; s.e. = 0.02%) and 8.3% (n = 9450 ripples over 4 datasets; s.e. = 0.06%) CA1 pyramidal cells are active during a ripple. Population burst size values greater than or equal to 10% occur 24 times as often in CA1 as in CA3 during ripples ($\geq$ 10% in 39.5% of ripples for CA1 and 1.65% of ripples for CA3, Fig. 2.7A(i)).

Next, we studied the average unit burst size inside and outside ripples for each pyramidal cell in both areas. We observed that the average unit burst size is significantly higher inside than outside ripples for CA3 neurons (CA3: average unit burst size outside ripples = 1.49 spikes/burst, s.e. = 0.02; inside ripples = 1.71 spikes/burst, s.e. = 0.04), but not for CA1 neurons (CA1: average unit burst size outside = 1.44 spikes/burst, s.e. = 0.01; inside = 1.45 spikes/burst, s.e. = 0.01; Fig. 2.7B).

2.4 Single-Unit Bursts in CA3 Predict CA1 Population Bursts

So far, we have characterized two independent observations in the two areas during ripples in SWS: more CA1 neurons become active, while individual CA3 neurons discharge more spikes. Since CA3 is thought to provide the dominant input to the CA3-CA1 circuit during SWS, it is natural to speculate if there is a causal relation-

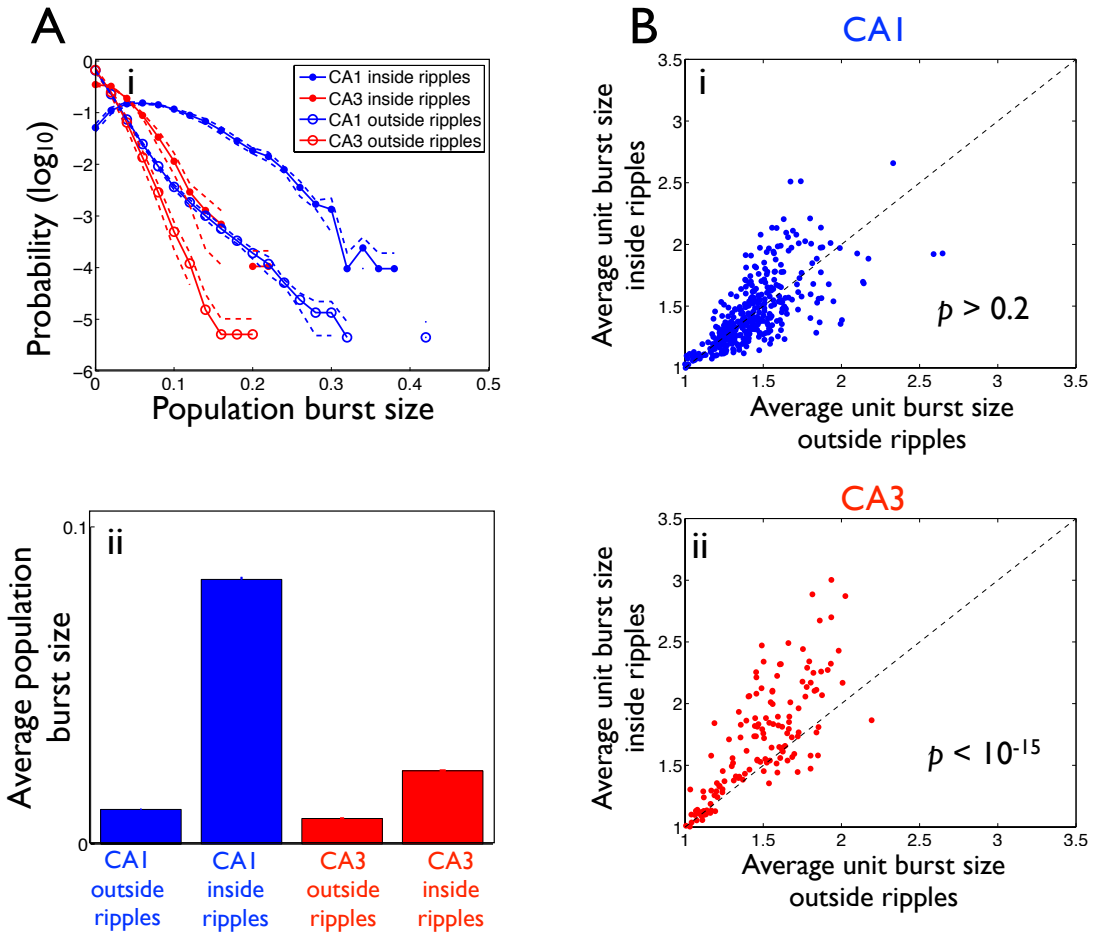

Figure 2.7: **Population burst size and unit burst size change in ripples. A (i):** Distributions of population burst sizes inside and outside ripples. Same datasets and sampling of neurons are used as in Figure 2.3B. Population burst size is calculated as the fraction of neurons that fire at least 1 spike within a 100 ms window around the ripple center (for the inside ripples case) or within a 100 ms window outside all ripples (for the outside ripples case). Note that population burst size is increased more from outside to inside ripples for CA1 than for CA3. **(ii):** The average population burst size outside and inside ripples for CA1 and CA3. Due to the large sample number, standard errors are very small and the errorbars are not visible in the plot. Note an ∼8 fold increase from outside to inside ripples for CA1 versus a ∼3 fold increase for CA3. **B:** Average unit burst size inside and outside ripples for individual pyramidal cells in CA1 (in blue) and CA3 (in red). Note the significantly higher values inside than outside ripples for CA3 neurons, but not for CA1 neurons. Only neurons that fire at least 50 spikes both inside and outside ripples are included. CA1: n = 370 cells. CA3: n = 140 cells.

ship between the two observations, i.e., bursts from a smaller coordinated set of CA3 neurons are responsible for launching population events involving many more neurons in CA1. If such a relationship exists, then bursting of individual CA3 neurons may play a special role in the CA3-CA1 transformation. We tested this hypothesis by investigating the relationships between CA3 bursts and CA1 activity in SWS. We performed our analysis on the basis of both spikes and LFPs.

At the spiking level, we found that bursts in CA3 are more effective than isolated single spikes in driving CA1 spiking. This observation was made in the following steps: We first separated all spikes from each CA3 neuron into two parts: isolated single spikes and spikes in bursts. We then treated the center of each burst as a single "spike". Depending on whether there are more isolated spikes or more bursts, we randomly down-sampled one of the resulting spike trains to ensure that the same number of events are used for computing cross-covariance with spikes from individual CA1 neurons (see Fig. 4.4 and Chapter 4 for details of down-sampling and cross-covariance analysis). We found that even when we treat spikes from each CA3 burst as a single "spike", compared to isolated single spikes, bursts from the same CA3 neuron have more coincidences with CA1 spikes (Fig. 2.8). Furthermore, on average CA3 bursts precede CA1 spiking (Fig. 2.8C(i)). In contrast, cross-covariances between isolated single spikes in CA3 and CA1 spikes peak at zero lag (Fig. 2.8B(i)).

We next studied if this extra effectiveness of CA3 bursts in driving CA1 spiking grows with the size of the CA3 bursts. This analysis is complicated by the fact that individual neurons do not have enough bursts of larger sizes for a meaningful comparison. To overcome this complication, for each dataset we built multiple time series, each consisting of first spikes of all bursts of the same size from all CA3 neurons. After equalizing the number of events used in each computation (see Fig. 4.4), we then calculated how many coincidences with CA1 spikes each of the time series has relative to single spikes. As is shown in Figure 2.9, on average larger bursts have more coincidences with CA1 spikes than smaller bursts. This difference is significant between bursts of size = 2 and bursts of size = 3 ($p < 0.005$, 1-sided paired t-test,

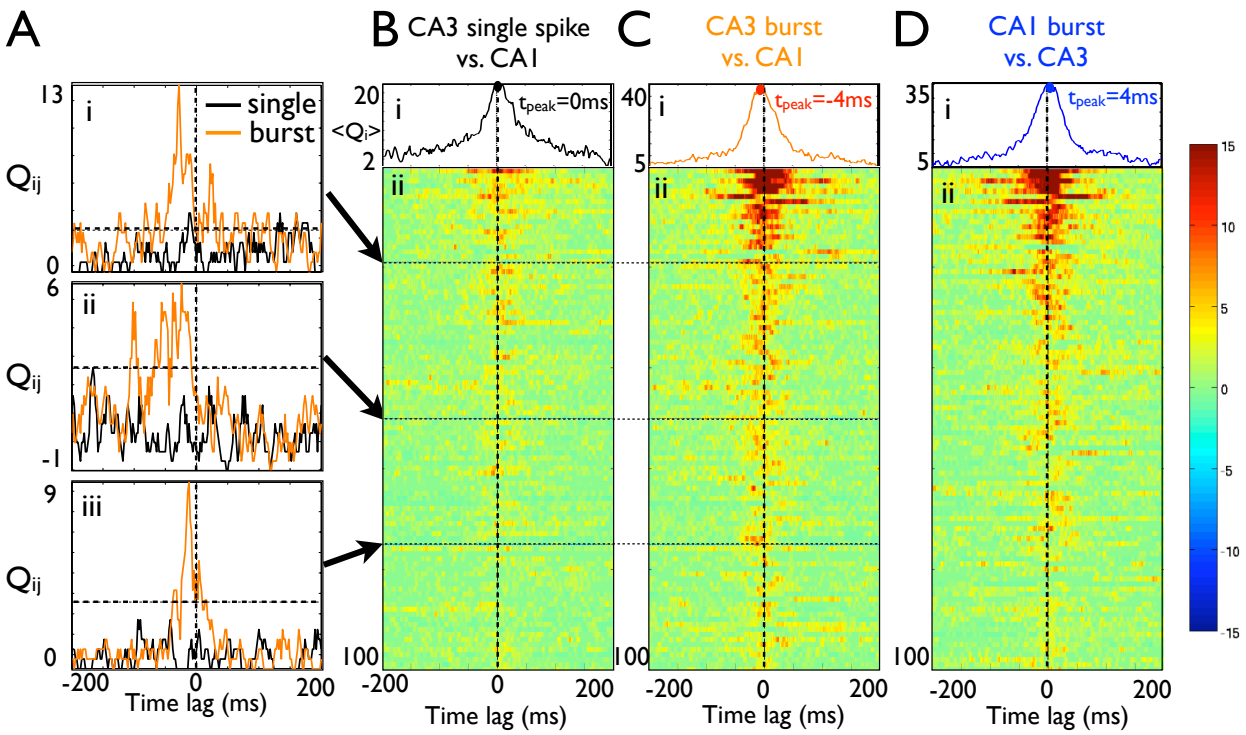

Figure 2.8: **Relationships between single spikes, bursts in CA3 and CA1 activity. A:** Three examples of standardized cross-covariance between isolated spikes from a CA3 neuron and all spikes from a CA1 neuron (in black), and between center of bursts from the same CA3 neuron and all spikes from the same CA1 neuron (in orange) during SWS. The same number of events go into the computation for the two scenarios, hence the cross-covariance values are directly comparable (see Chapter 4 and Fig. 4.4 for more details). Horizontal dashed line indicate significance at $p = 0.01$ level. Note that the number of coincidences is higher for bursts. The peaks occur to the left of zero lag, indicating that CA3 bursts tend to precede CA1 firing. **B: (ii)** Each row shows the standardized cross-covariance between isolated spikes of a CA3 neuron and all spikes of a CA1 neuron. The top 100 pairs ordered by peak value are plotted. **(i)** The standardized mean cross-covariance. Note the peak has zero lag. **C:** Same as **B**, but for center of bursts in CA3. Cell pairs are shown in the same order as in **B**(ii). Note the peak in i) is at -4 ms lag, indicating that CA3 bursts precede CA1 spiking. **D:** Same as **C**, but for center of bursts in CA1 vs. all spikes in CA3. Note the peak has 4 ms lag, indicating that the timing relationship shown in **C**(i) is not an artifact from using centers of bursts.

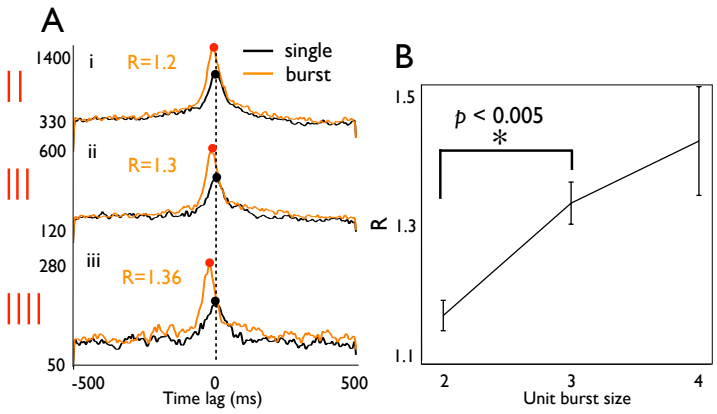

Figure 2.9: **Relationship of CA3 unit burst size and CA1 activity. A: (i-iii)** Cross-covariance in raw counts between isolated CA3 spikes and all CA1 spikes (in black), and between first spikes of CA3 bursts of different sizes and all CA1 spikes (in orange). For each burst size, the same number of CA3 spiking events go into the computation for the two scenarios. For each scenario, a quantity E is calculated as the peak divided by background count. To compare the effectiveness of bursts and isolated spikes of CA3 in driving CA1 activity, R is calculated as E_{burst}/E_{single}. Note that as burst size increases, R increases, suggesting that larger CA3 bursts are more effective in driving CA1 activity. **B:** The relationship between R and unit burst size. R is significantly different between burst size = 2 and burst size = 3. $p < 0.005$, 1-sided paired t-test. n = 5 datasets.

Fig. 2.9B).

In summary, there is a positive relationship between sizes of CA3 bursts and their effectiveness in driving CA1 spiking. However, we wished to rule out the possibility that CA1 spiking activity might be over-represented by spikes from a small number of tetrodes sampling from a large number of neurons, because spikes detected from a few tetrodes may not be an accurate readout of the global activity level in CA1. Since ripples are network events detectable on all CA1 tetrodes (Fig. 1.4) and there exists a positive relationship between population firing rate and LFP amplitude filtered in the ripple band (Fig. 2.1B(iii)), the CA1 LFP signals can be a more robust measure of global CA1 activity level (Fig. 2.1B(iii)). Therefore, we next characterized the influence of CA3 bursts on CA1 activity at the LFP level. Figure 2.10A(i-vii) shows the timing relationship between burst onset and ripple onset for CA3 bursts of different sizes. As burst size increases, CA3 neurons fire progressively earlier with respect to the onset of ripples (Fig. 2.10A(viii)). Furthermore, larger bursts in CA3 correspond

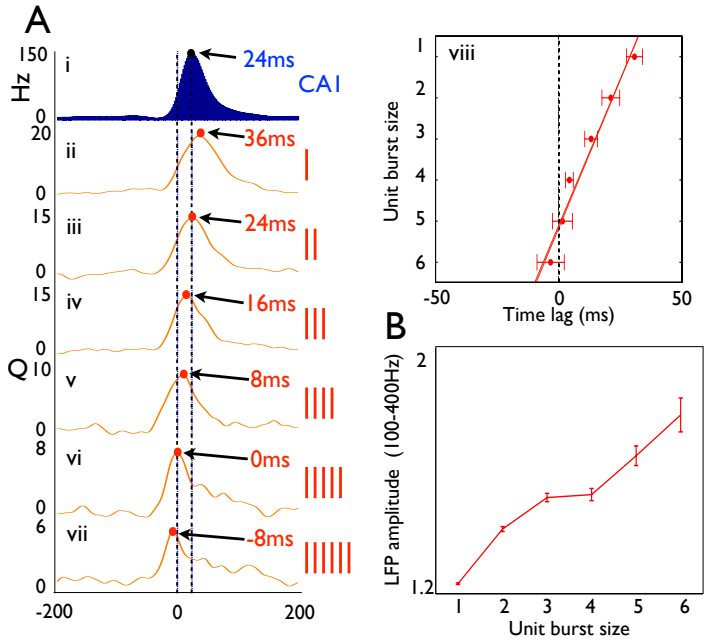

Figure 2.10: **Timing relationship between bursts and ripple onsets. A: (i)** CA1 multiunit firing rate aligned to ripple onset. A ripple's onset is defined as the first time when the power of filtered LFPs reaches 2 std above the mean across all CA1 tetrodes. Note in this dataset most CA1 spikes occur after ripple onset (at zero-lag), with the peak at +24 ms. **(ii-vii)** Standardized cross-covariance between first spikes of all CA3 bursts of difference sizes and ripple onsets. Note that as burst size increases, CA3 fires progressively earlier with respect to ripple onset. This relationship is also shown in (viii), which combines 5 datasets. **B:** The relationship between unit burst size and CA1 LFP amplitude filtered in ripple band. We calculate the mean LFP amplitude within a 100 ms window around each burst's center, divided by its time average during SWS. Note that larger bursts correspond to larger oscillations. This result is independent of the threshold used for ripple identification.

to larger oscillations in the ripple band in CA1 LFPs (Fig. 2.10B). Both of these observations provide additional experimental support for the hypothesis that CA3 bursts play a crucial role in launching population events in CA1.

Chapter 3

Discussion

3.1 Nonlinear CA3-CA1 Transformation during SWS

Our observations suggest that during SWS, CA1 acts as a selective amplifier of CA3 activity. When the CA3 population firing rate is relatively low, CA1 firing rates do not co-vary with those of their CA3 inputs. Once the CA3 population firing rate exceeds twice its background level, however, CA1 amplifies CA3 input, which is often manifested as a population burst accompanied by a ripple in the LFP (Fig. 2.1B). Furthermore, these population firing rate increases are implemented differently in the two areas. While population burst size increases during ripples for both CA1 and CA3, significantly more CA1 neurons than CA3 neurons become active during ripples (Fig. 2.7A). On the other hand, individual CA3 neurons discharge more spikes than CA1 neurons (Fig. 2.7B). As we elaborate below, these differences in network activity patterns between the two areas relate directly to the nonlinear transformation of CA3 input by CA1 and have important consequences for the functional roles of the CA3-CA1 circuit in memory formation.

3.2 Implementation of a Selective Amplifier of CA3 Activity by CA1

It has been previously proposed that unreliable synapses with short-term facilitation properties can be viewed as filters that transmit bursts but filter out single spikes[43]. We argue that the CA3-CA1 circuit may implement this filter, due to its characteristic anatomical and physiological properties. In particular, here we have shown that during SWS, CA3 pyramidal cells fire both isolated spikes as well as prolonged bursts (Fig. 2.6B). Previous studies have demonstrated that the Schaffer collateral synapses are both unreliable and can be facilitated. We argue that these physiological properties, combined with the highly extensive projection from CA3 to CA1, may be sufficient to provide the mechanism responsible for the CA3-CA1 transformation we describe.

The unreliability of the Schaffer collateral synapse is well-established experimentally[44,45]. A typical CA3-CA1 synapse can have a *success rate* as low as 0.1 (Fig. 3.1A), i.e., out of ten isolated presynaptic spikes, only one of them leads to vesicle release at the presynaptic terminal. Furthermore, CA3-CA1 synapses have only about one-tenth the potency of synapses connecting two CA3 pyramidal cells. The average unitary EPSP is 0.6-1.3 mV at CA3-CA3 synapses[46], but only 0.13 mV at CA3-CA1 synapses[47]. We propose that the unreliability and weakness of CA3-CA1 synapses ensures that isolated background CA3 spikes are not transmitted to cortical targets and thus CA1 attenuates CA3 input under these circumstances (Fig. 3.2).

On the other hand, CA3-CA1 synapses undergo strong presynaptic paired-pulse facilitation (PPF) in response to multiple presynaptic CA3 action potentials with short ISIs[48,49,50]. The average postsynaptic response to the second of a pair of stimuli is facilitated, peaking at around 20ms after the first spike[51]. Furthermore, in contrast to the very low success rates in response to single isolated spikes from CA3, short-term facilitation significantly increases the success rate for bursts[52,48]. At certain CA3-CA1 synapses, a two-spike burst can almost guarantee vesicle release (Fig. 3.1B).

Therefore, when multiple bursts from a few CA3 neurons reach a postsynaptic

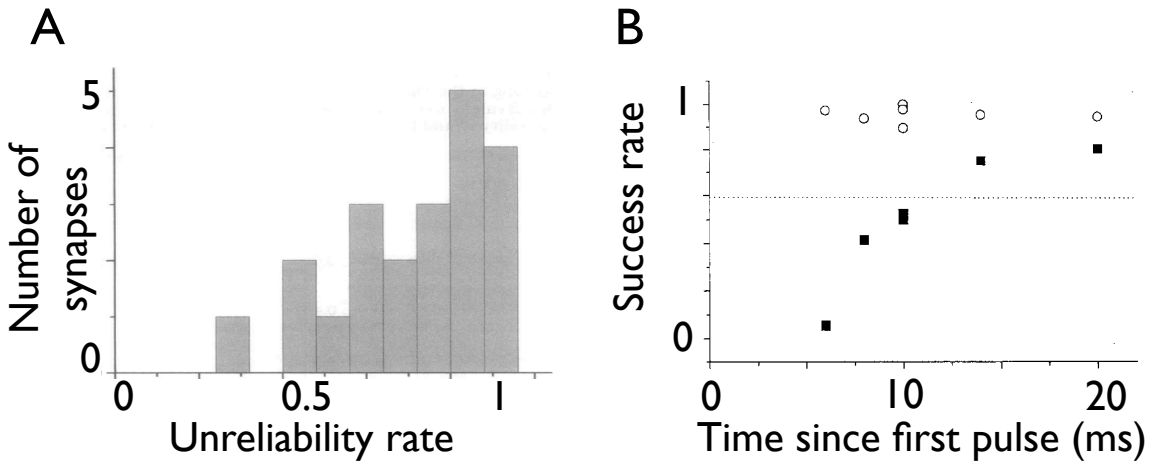

Figure 3.1: **Short-term facilitation at unreliable CA3-CA1 synapses. A:** CA3-CA1 synapses are highly unreliable. *Success rate* is calculated as the probability of vesicle release in response to a presynaptic input. *Unreliability rate* is 1 - *success rate*. Note that the majority of synapses have unreliability rates above 0.6. Also note that the average unreliability rate is likely to be underestimated for two reasons: 1) Experiments are performed under the minimal stimulation protocol, which can undercount the number of synapses being stimulated, and 2) only synapses with success rate $\geq$ 5% are included, which can bias sampling toward more reliable synapses. Adapted from[44]. **B:** Success rates at a CA3-CA1 synapse for the second stimulus in a pair as a function of time since the first stimulus. Open circles: success rates when no EPSC was evoked by the first stimulus. Closed squares: success rates when a release occurred in response to the first stimulus. The initial depression to a second stimulus when the first stimulus triggers release is due to time required for a vesicle release site to be refilled. Horizontal dotted line: the release probability for the first stimulus. Note facilitation almost guarantees vesicle release in response to a pair of two stimuli less than 20ms apart. Adapted from[48].

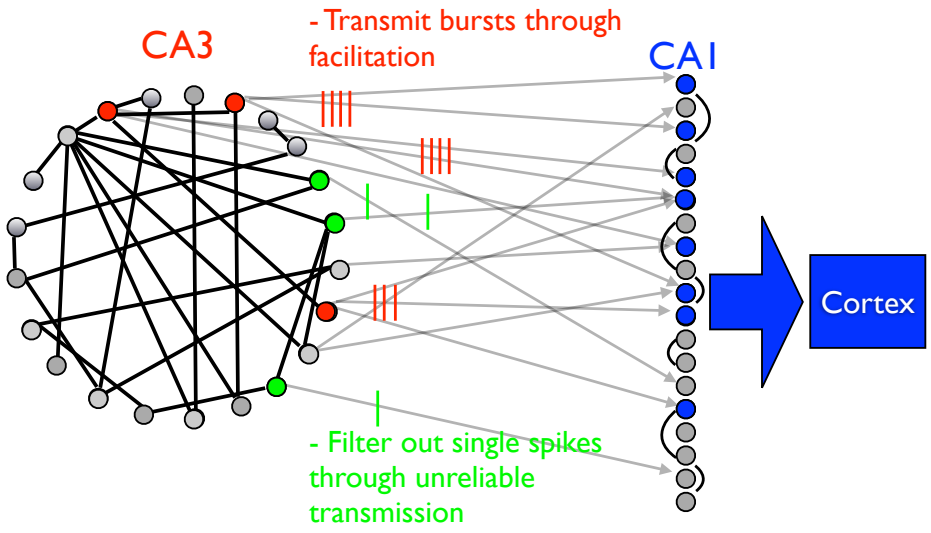

Figure 3.2: **Roles of CA3 bursts in influencing CA1 activity.** Compared to CA3-CA3 synapses, CA3-CA1 synapses are unreliable (shown as lighter color of the lines connecting CA3 to CA1 neurons). This allows CA1 to filter out single isolated spikes from CA3, and transmit only bursts through. Bursts are effective, thanks to short-term facilitation at CA3-CA1 synapses.

CA1 neuron, the CA1 neuron will respond much more strongly than if it had received the same number of single spikes from multiple CA3 afferents. Since CA3 neurons project extensively to CA1, with any single CA3 neuron contacting up to 10,000 CA1 neurons[12] (see Chapter 1), it is likely that coordinated bursts from a small group of CA3 neurons are sufficient to influence enough CA1 neurons to briefly push the entire CA1 network into a synchronous, high-firing ripple mode, and thus achieve a nonlinear amplification of CA3 input by CA1.

3.3 Role of CA3 Bursts in Shaping CA3-CA1 Circuit Activity

According to the implementation mechanisms hypothesized above, CA3 bursts increase the success rate of unreliable CA3-CA1 synapses nonlinearly through short-term facilitation. We have shown that the increase of CA3 unit burst size and the

launching of CA1 population events co-occur with hippocampal ripples (Fig. 2.7). Furthermore, CA3 bursts predict and precede CA1 responses (Fig. 2.8, Fig. 2.10). These observations, as well as anatomical and physiological features of the CA3-CA1 circuit discussed earlier in this chapter, suggest that CA3 bursts may play a crucial role in shaping CA3 and CA1 activity during SWS, as discussed in more detail below.

CA3 bursts may be essential in ensuring reliable transmission of activity to CA1 and beyond, while maintaining overall sparse firing patterns within CA3. Relatively sparse firing in CA3 is probably necessary to avoid runaway excitation and epileptiform activity in this densely recurrent circuit. Furthermore, as area CA3 is believed to act as an autoassociative network, sparse firing patterns minimize overlap between the representations of distinct memory traces[53]. On the other hand, despite the highly unreliable CA3-CA1 synapses, it is important that certain neuronal activity patterns in CA3 be reliably transferred to CA1, since CA1 serves as the only anatomical "gateway" between CA3 and the neocortex (Fig. 1.2). These two requirements of CA3 activity, sparse firing and reliable transmission, can be simultaneously satisfied by CA3 bursts, which through facilitation can reliably trigger CA1 responses, while still maintaining a relatively small set of neurons within CA3 active at any given time.

In addition to possibly launching population events in CA1, CA3 bursts may also play an essential role in shaping the patterns of firing within these population events. Previous studies have shown that neuronal firing across multiple CA1 neurons is replayed during ripples in SWS following awake experience[54]. This suggests that CA1 may not only act as an amplifier of CA3 input, but also transform CA3 neuronal representations into a format, i.e., through cell membership, amount, and ordering of firing, that is parsable by downstream cortical targets. One of the most robust protocols for the induction of long-term potentiation (LTP) is high-frequency stimulation of the Schaffer collateral pathway[55,56]. It is interesting to note that the frequency of such stimulation is similar to the bursting frequency of CA3 neurons. Therefore, CA3 bursts may serve to induce LTP at specific CA3-CA1 synapses. It is likely that by modifying the efficacy of specific CA3-CA1 synapses, CA3 bursts can not only adjust what types

of CA3 input trigger ripples, but also fine tune the cell membership and ordering of firing across CA1 neurons during ripples. All these processes will be critical for the reliable transfer of relevant CA3 neuronal patterns to the neocortex. Such a role for CA3 bursts in plasticity is strongly supported by a recent *in vitro* demonstration that the same high-frequency stimulation protocol that induces LTP also induces ripples[57].

Finally, CA3 bursts may facilitate synaptic changes within CA3 itself. Weak presynaptic stimulation alone normally fails to induce LTP. However, under certain circumstances, when weak presynaptic stimulation co-occurs with postsynaptic bursts, LTP could be induced[58]. Therefore, as a result of the recurrent connections within CA3, bursting activity may lead to epochs of intense synaptic modification. Some theoretical and experimental studies have provided evidence in support of this idea. For example, synchronous bursts within CA3 have been hypothesized to promote the self-organization of spontaneous network activity patterns within CA3, that fall on the border between random spiking and synchronous bursting[59].

3.4 Role of CA3-CA1 Circuit in Memory Formation

According to the predominant two-stage model of memory formation, memories are first encoded within the hippocampus during awake before being gradually consolidated across neocortex during sleep[60,61,62,63,64]. In this framework, the recurrent synapses of CA3 are believed to be the storage site for the initial memory traces. Details of how these memory traces undergo further reorganization within CA3 as well as how they are transferred to the neocortex are still unknown. Our study provides insights on how a nonlinear CA3-CA1 transformation can facilitate these processes.

If CA3 functions as an autoassociative network, then each of the memory traces stored in it may be represented by an attractor of the network. The CA3 network state at any given time during SWS can be summarized by a set of synaptic weights. Memory traces are reorganized within CA3 by adjustments to these weights triggered by spontaneous CA3 activity. Theoretical work has shown that activity patterns in

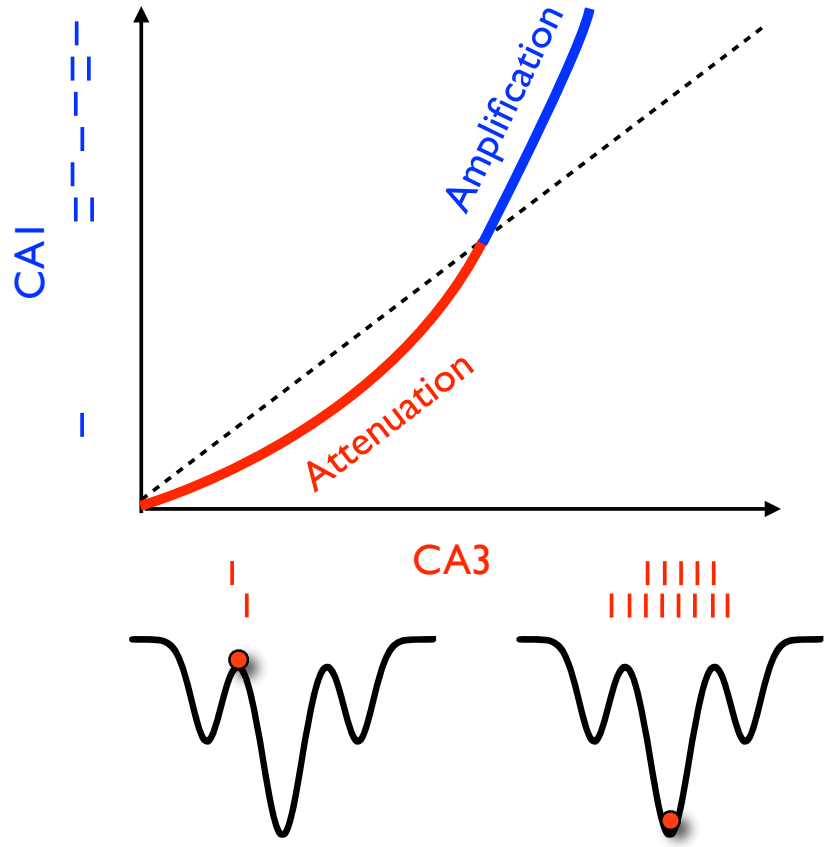

Figure 3.3: **CA3-CA1 transformation during SWS.** CA1 attenuates weaker isolated CA3 spikes, which represent intermediate states in-between attractors in the associative network, but launches population events involving many neurons at stronger CA3 bursting input, which reflects convergence to network attractors.

recurrent networks consist of two distinct states: attractor states, where the network settles into a relatively high-firing rate mode while resisting the effects of small external perturbations, and intermediate states, where the network moves transiently between attractors while firing at a relatively lower rate. Distinct attractor states are thought to correspond to distinct memory traces. It is important that CA1 responds to the two network states differently. For activity that represents intermediate states, CA1 should not act as a relay to the neocortex, as this activity does not correspond to a *bona fide* memory trace. Activity that underlies convergence to network attractors, however, should be reliably transferred and, if possible, amplified by CA1 to neocortex, as it relates to memory traces to be permanently stored in the neocortex.

If we hypothesize that coordinated bursts in CA3 reflect convergence to an attractor of the CA3 network, then thanks to the amplification segment of the nonlinear CA3-CA1 transformation, representation contained in this attractor will be preferentially amplified by CA1 to the neocortex (Fig. 3.3, blue segment). Selectively replaying patterns stored in the hippocampus may lead to gradual strengthening of downstream cortical traces, a process that may underlie memory consolidation. Previous evidence indicates that it can take up to several weeks for recent memories, stored in the hippocampus, to become long-term memory, stored in the neocortex. Therefore, the replay of CA3 neuronal patterns may occur many times in numerous SWS epochs across multiple days. Furthermore, this paradigm allows multiple memory traces within CA3 to be transferred to the neocortex simultaneously, as different population events (ripples) in CA1 can have different firing patterns triggered by convergence to different CA3 network attractors.

On the other hand, thanks to the attenuation segment of the same nonlinear CA3-CA1 transformation, intermediate network states, hypothesized to be reflected by isolated background spikes, are less likely to be transmitted by CA1 to the neocortex (Fig. 3.3, red segment). During these circumstances, synaptic plasticity changes can be gradually induced within CA3, without affecting activity in downstream structures. In this way, the CA3-CA1 circuit can selectively transfer stable neuronal representations

in CA3 through to the neocortex and at the same time minimize any influence exerted from intermediate states in CA3.

Chapter 4

Methods

4.1 Electrophysiological Recordings

Electrophysiological signals were acquired using tetrode recordings [65]. Five male Long-Evans rats (age 3-5 months, weight 350-450g) were implanted with a custom-built microdrive array allowing the independent adjustment of 24 individual tetrodes. In two of the animals, all tetrodes targeted CA1 pyramidal layer. In the other three animals, 6-12 tetrodes targeted CA1 and 6-12 tetrodes targeted CA3 pyramidal layers. Individual tetrodes were gradually lowered to their targets over several days and further micro-adjusted to optimize yield and stability. Each tetrode signal was buffered by a unity-gain headstage preamplifier and further differentially amplified with a gain of 2000. The broadband amplified signals were digitally acquired at 25K Hz as 24-bit samples (National Instruments PXI-4472) and stored to disk using custom acquisition software that we developed. Three light-emitting diodes were fixed to the top of the microdrive array to allow tracking of the animal's position from video recordings captured at 30 frames per second. Each video frame was timestamped by the acquisition system in order to synchronize position and neuronal data. All recordings were conducted in a sleep box that was highly familiar to the animal immediately after the animal had performed a variety of spatial tasks (linear track traversals, T-maze). The animal stayed in the sleep box for 2-10 hours, sleeping during most of the time, before starting the next spatial task. All animal procedures were done in accordance with

NIH guidelines and with approval of the Caltech Institutional Animal Care and Use Committee.

4.2 Spike and Local Field Potential Analysis

Spikes and LFP traces were obtained by digitally filtering the broadband signal. For spikes, a bandpass filter was designed using the Parks-McClellan algorithm with transition bands of 500 – 600 Hz and 6000 – 6100 Hz and maximal ripple of 10^{-5} in the stopband and 10^{-3} in the passband. LFPs were computed by downsampling the broadband signal by a factor of 12 in three stages (2, 2, 3); each stage used a 500-tap FIR linear-phase lowpass filter designed using the window method. Spikes were clustered into single units on the basis of their amplitudes recorded on each of the four tetrode channels (Fig. 4.1). Units with firing rate less than 1 Hz in the entire recorded session were classified as pyramidal cells.

4.3 Ripple Identification

One channel of each CA1 tetrode was selected. LFP from that channel was filtered between 80 – 400 Hz using Parks-McClellan FIR filters. Candidate events were identified as deviations in the power of the filtered traces that exceeded two std's of the filtered signal. From this set artifact events were rejected based on the duration (< 10 ms), LFP frequency content (< 100 Hz), relative power in gamma (40 – 80 Hz) and ripple bands (ripple power / gama power < 1.6) and amplitude associated with each candidate event ($< 50\%$ from the minimum to the mode of the amplitude value distribution). A global ripple was determined as candidate events that were consistently detected across multiple CA1 tetrodes. A variety of ripple bands and thresholding parameters were tried, and none of the main results depended on how the parameters were chosen.

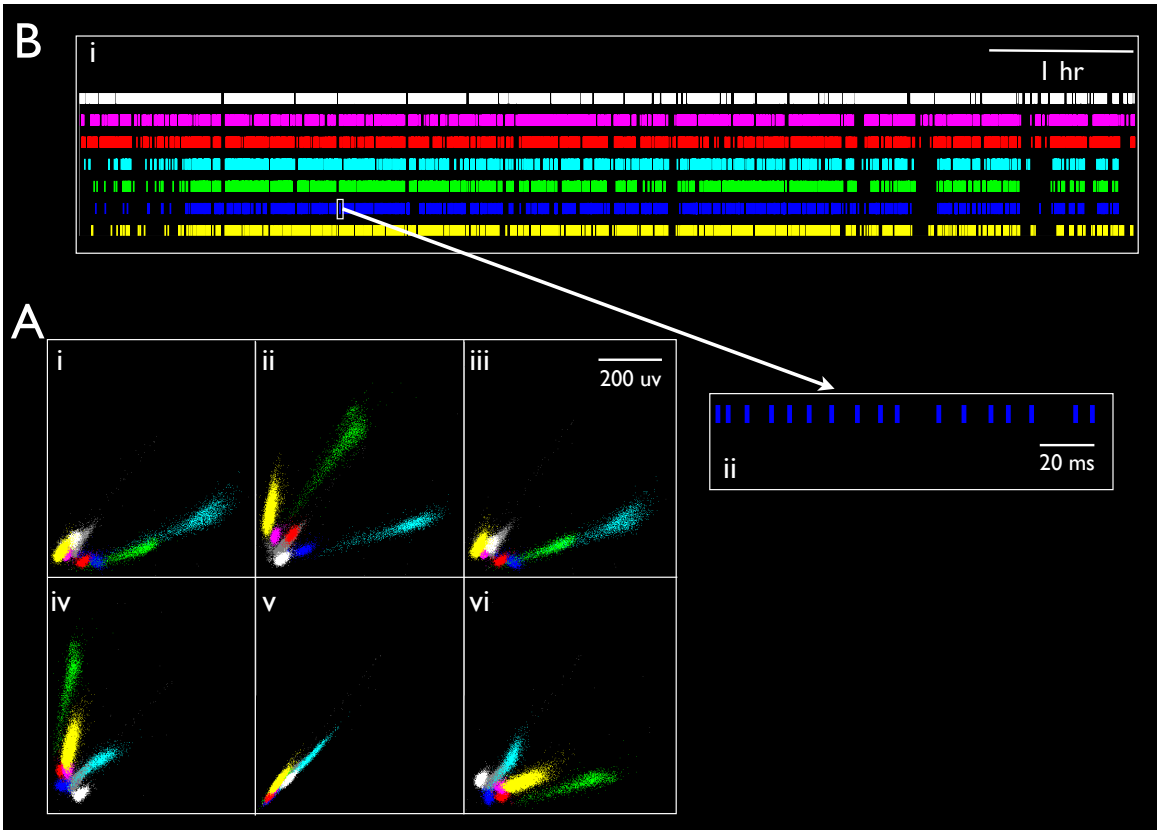

Figure 4.1: **Single unit clustering of spikes from a CA3 tetrode. A: (i)-(vi)** Each dot represents the peak amplitude of a spike on two of the four tetrode channels. This gives rise to a total of 6 different projections. In this 4D amplitude space, spikes can then be assigned to individual clusters, each of which includes spikes from a same cell. 7 clusters can be isolated from this tetrode and are shown in different colors. Spikes that cannot be assigned to any cluster are shown in gray (those bottom left dots along the diagonal line). All spikes are shown. Note that the cyan and green clusters are very close in (i, iii), but are far apart in (ii, iv, vi). **B: (i)** Rasters of the clusters in (A). Spikes from the same cluster have the same color as in (A). **(ii)** An example of a long burst (17 spikes in 140 ms).

4.4 Burst Identification

Auto-correlation of spike time shows that ISIs during a burst can be as short as 4 ms (Fig. 4.2A(iii)). The average auto-correlation trace peaks at ± 5 ms and gradually decreases to baseline without showing a second mode. The timing profile is similar for both CA1 and CA3 cells (Fig. 4.2B). Bursts were defined as a sequence of any number of consecutive spikes with ISI $\leq$ 20 ms.

Some CA1 and CA3 cells are less likely to burst than others (Fig. 2.6). We confirmed that this is not a result of difference in tetrode positions by showing that cells on the same tetrode can have very different bursting properties (Fig. 4.3).

4.5 Cross-Covariance Analysis

Cross-covariance between two cells was first computed as raw spike counts. These counts were then normalized to unit normal Z-scores at each lag. This resulted in a *standardized cross-covariance*. A *standardized mean cross-covariance* across multiple cell pairs was computed by summing the standardized cross-covariances between all pairs and dividing by the square-root of the number of pairs. Refer to [66] for details of this computation.

4.6 Bursts vs Single Spikes Comparison

When comparing single spikes vs bursts from CA3 cells in their cross-covariance with CA1 spikes, we took special care to ensure that the same number of events were used. For each cell (Fig. 2.8) or dataset (Fig. 2.9), time series of bursts onsets or centers were constructed (Fig. 4.4). Between this time series and the one consisting of only isolated single spikes, the one with more number of events was randomly resampled to match their number of counts. For comparison among bursts of different sizes (Fig. 2.9), time series consisting of first spike of bursts of different sizes were used

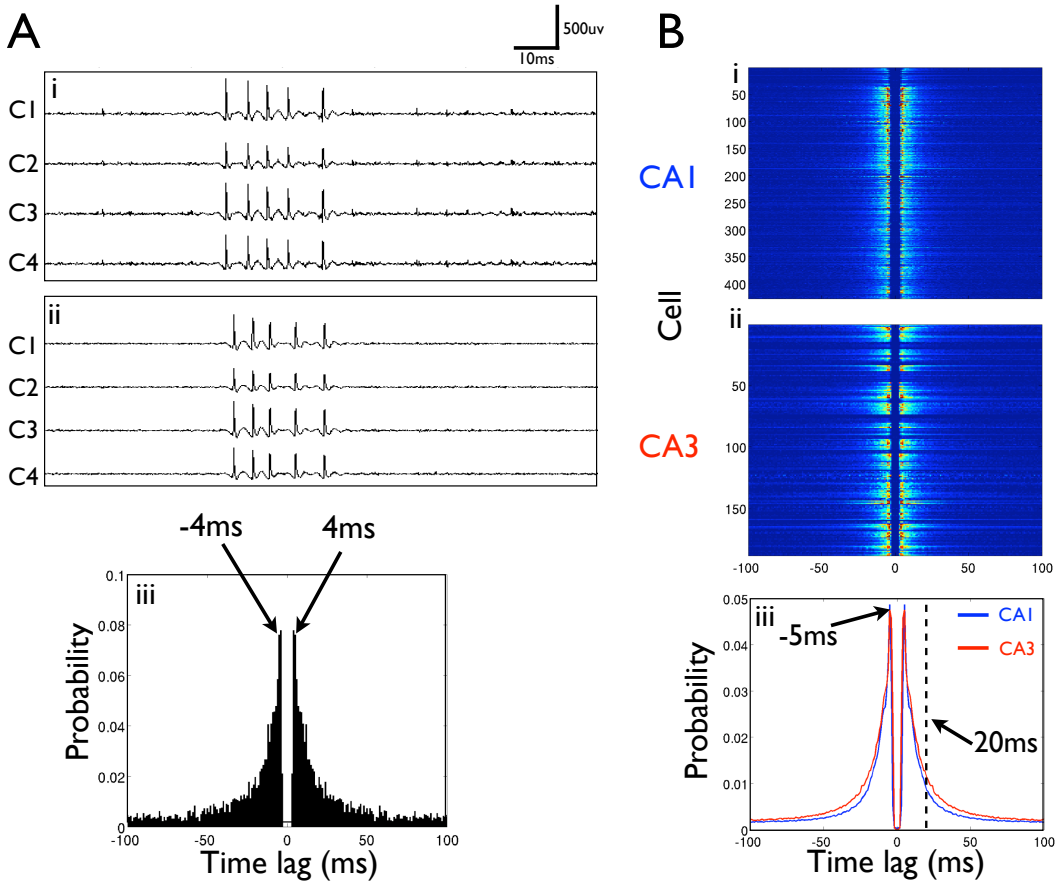

Figure 4.2: **Bursts in the hippocampus. A: (i)** A burst of 5 spikes from a CA3 neuron detected on 4 tetrode channels. Note the small interspike interval and decrease in amplitude from the 1^{st} spike. **(ii)** Another burst of 5 spikes from the same cell but 1hr later. Note the similar amplitude and timing profile to (i). **(iii)** Auto-correlation of spikes from the cell in (i,ii) during SWS. Note a sharp peak at $\pm$4 ms followed by a gradual decrease to baseline. **B: (i,ii)** Each row represents an auto-correlation of spikes from one cell, normalized by the peak value. CA1: n = 427 cells. CA3: n = 188 cells. **(iii)** Mean of (i, ii). Note sharp peaks at $\pm$5 ms and similar profile for CA1 and CA3 cells. We used 20 ms as the ISI threshold for burst identification. A few other thresholds (10 ms, 25 ms, 50 ms) were also tried and none of the main results were affected.

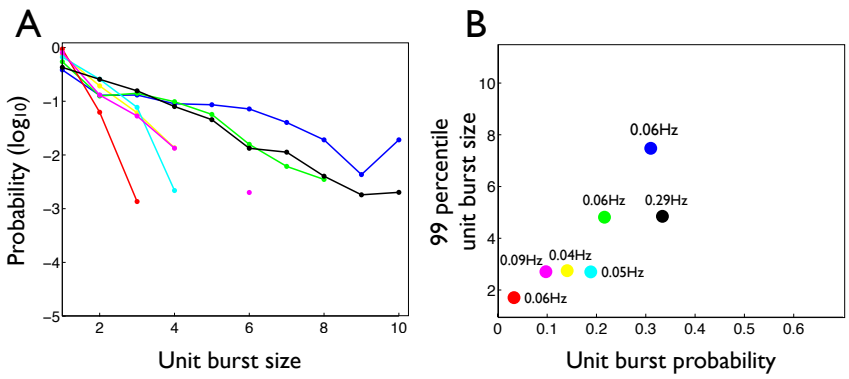

Figure 4.3: **Different burst properties of cells on the same tetrode. A:** Distributions of unit burst sizes for the 7 cells in Figure 4.1. The cell in white in Fig. 4.1 is plotted in black here. All other cells are plotted in the same color. **B:** Unit burst probability and 99th percentile unit burst size of the same 7 cells. Note the blue cell and the red cell have the same firing rate but very different bursting properties. Cells localized around the tip of the same tetrode can have very different tendencies to discharge bursts.

and the same procedure was applied after that.

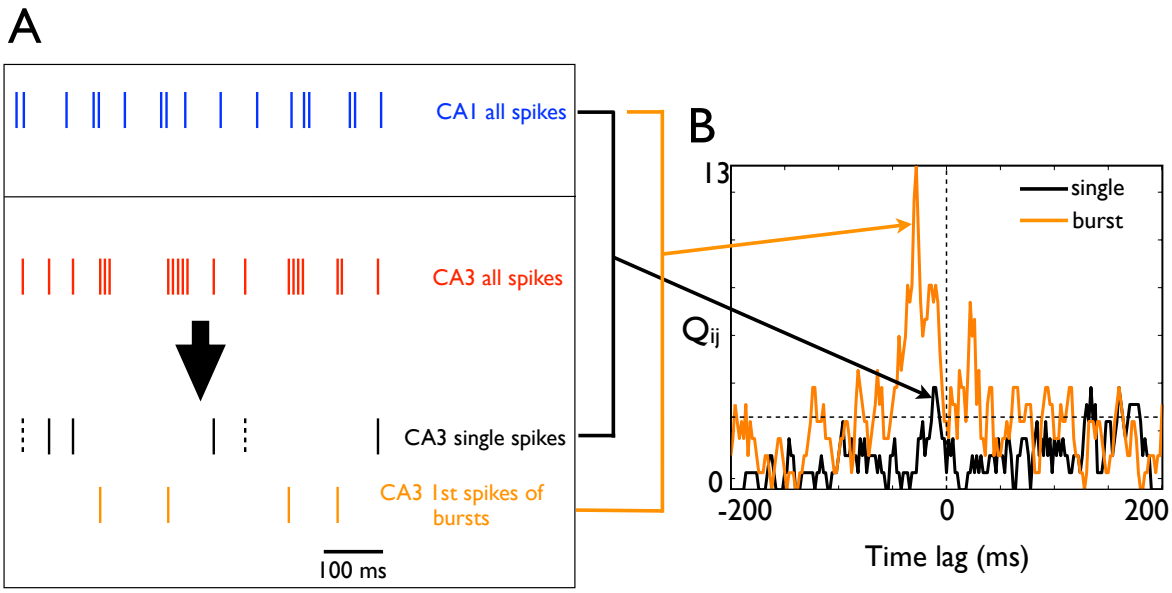

Figure 4.4: **Computing standardized cross-covariance between CA1 and single spikes or first spikes of bursts of CA3. A:** Steps to compare the effect of isolated single spikes and bursts of CA3 on CA1 firing. Spikes of a CA3 cell are first parsed into two time series: isolated single spikes and first spikes of bursts of size ≥ 2. The one with the larger number of spikes is then randomly downsampled to match the number of spikes in the two series (illustrated as the dashed spikes). **B:** Standardized cross-covariance between each of the two derived series in (A) and CA1 spikes is computed. Note that to obtain a meaningful comparison of the two series, the same number of events from each goes into the cross-covariance computation.

Chapter 5

Supplementary materials

5.1 Controlling for Single-Unit Clustering Quality

The results of our analysis could be complicated by imperfect clustering of single units[67]. To address this concern, we applied the following controls. First, an isolation distance (ISO) was computed for each neuron according to[68]. ISO estimates how well-separated the spikes of one cluster are from other spikes recorded simultaneously on the same tetrode[68]. We noted that there is no significant correlation between a neuron's ISO value and its likelihood to fire bursts (Fig. 5.1). We then re-performed part of our analysis that involves single-unit data using pyramidal cells whose ISO's exceeded different minimal levels. Finally, analysis was performed on a small selection of well-separated neurons that we hand picked (28 CA1 units and 20 CA3 units. See Appendix for statistics and cluster plots of these neurons). It was confirmed that our main results remain qualitatively unchanged independent of the clustering quality. (Fig. 5.2, Fig. 5.3, Fig. 5.4, Fig. 5.5).

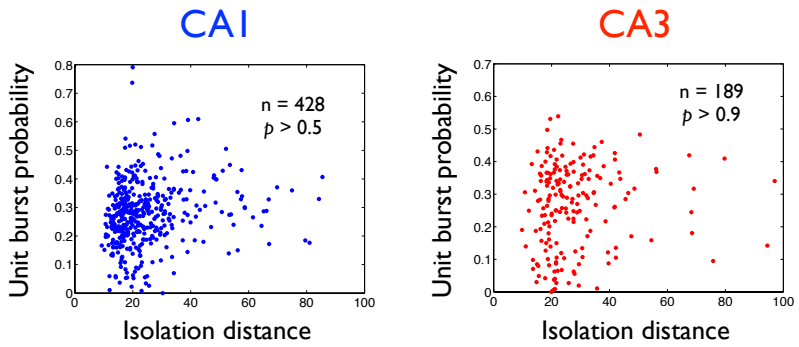

Figure 5.1: **Isolation Distance vs. Burst probability.** Note a neuron's ISO does not correlate with its likelihood to fire bursts.

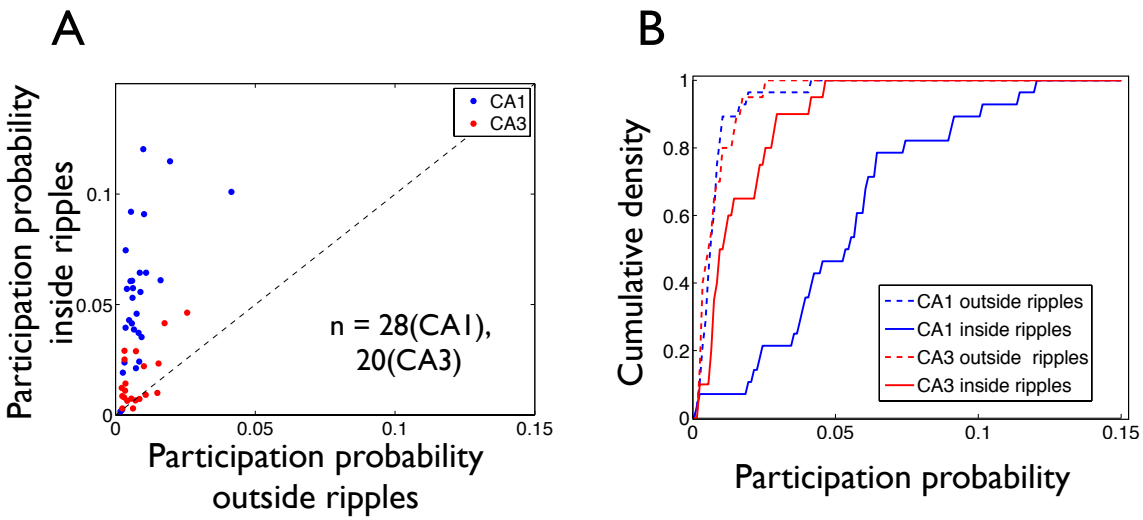

Figure 5.2: **Participation probability outside and insider ripples of highly separable pyramidal cells. A:** Participation probability of neurons that were hand picked for their high separability. Participation probability inside ripples is computed as the probability of firing at least 1 spike within a 100 ms window around the center of ripples. Participation probability outside ripples is computed as the probability of firing at least 1 spike within any 100 ms window outside of all ripples. Each dot represents one neuron. Note that while CA1 (blue) and CA3 (red) neurons have similar participation probability outside ripples, it is increased significantly more inside ripples for CA1 neurons than for CA3 neurons. n = 28 CA1 units, 20 CA3 units. **B:** Cumulative density plots for (A). Note the small difference between CA1 and CA3 outside ripples, but large difference inside ripples.

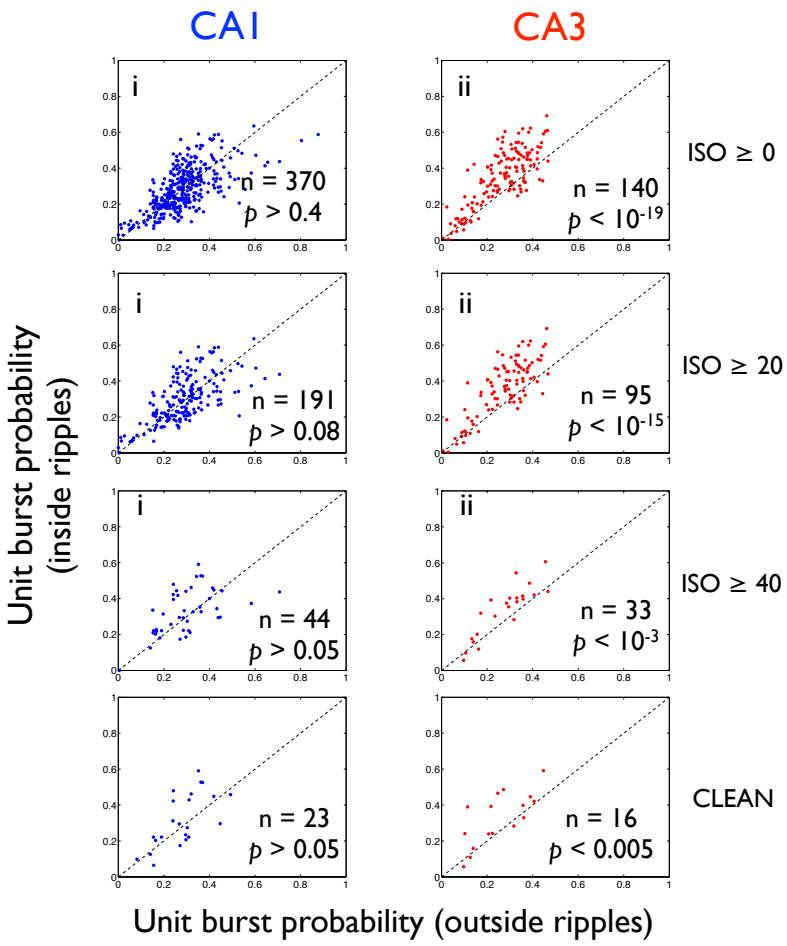

Figure 5.3: **Uni burst probability of neurons of varying separability.** Unit burst probability outside (x-axis) and inside (y-axis) ripples for individual CA1 and CA3 neurons of varying separability. Top to bottom, neurons with different minimal ISO. The bottom most row are for neurons that were hand picked for their high separability. Note that regardless of which ISO threshold is used, the unit burst probability is increased from outside to inside ripples more for CA3 neurons than for CA1 neurons.

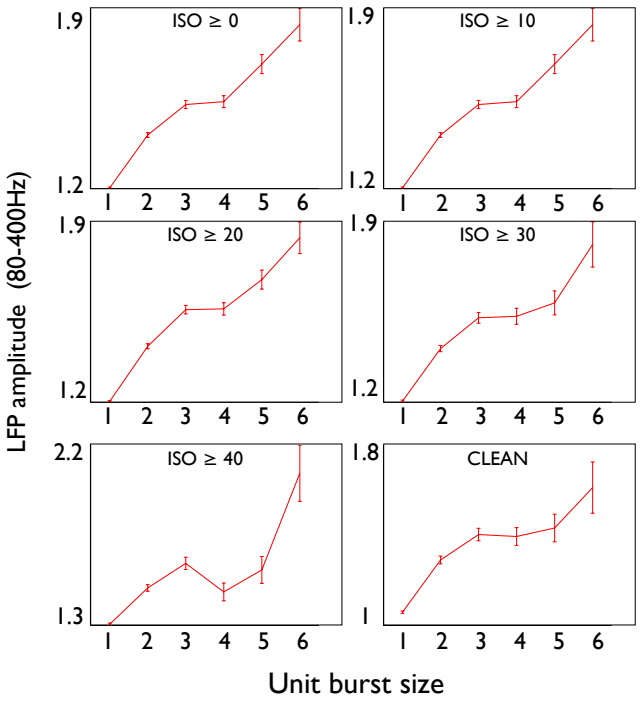

Figure 5.4: **The relationship between unit burst size and LFP amplitude filtered in ripple band for neurons of varying separability.** Note that regardless of ISO threshold, there remains a positive relationship between unit burst size and LFP amplitude.

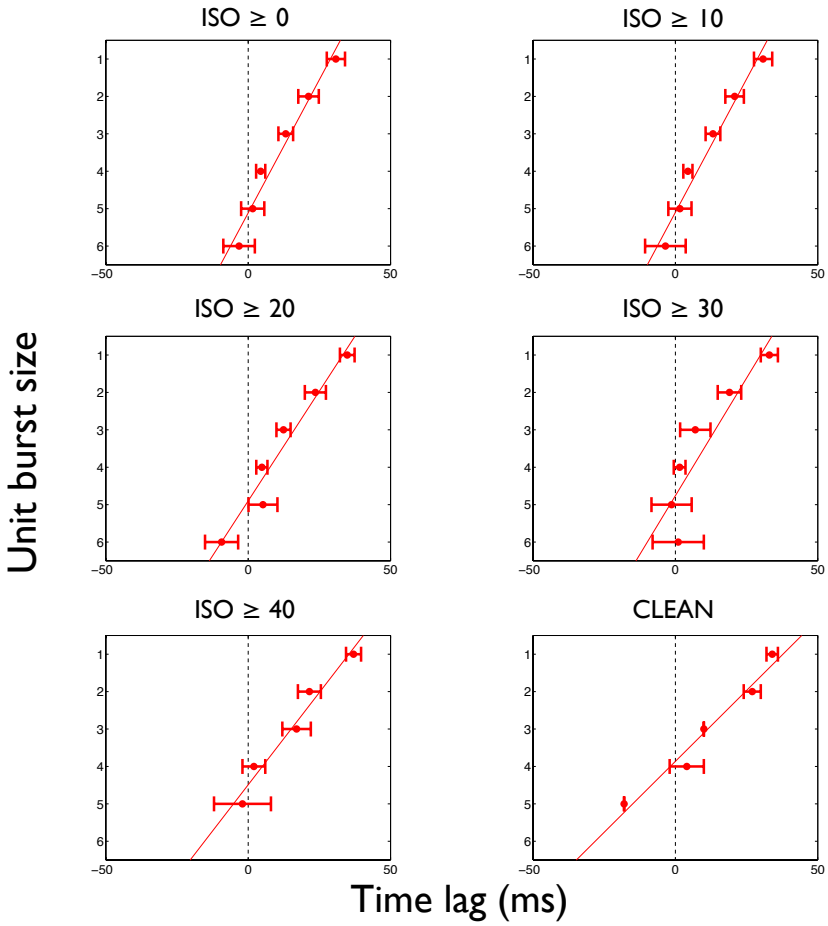

Figure 5.5: **Timing relationship between bursts and ripple onsets for neurons of varying separability.** Note that regardless of ISO threshold, as unit burst size increases, CA3 fires earlier with respect to ripple onset.

Chapter 6

Appendix

The following are firing properties in table format and cluster plots of all hand picked pyramidal cells used in chapter 5. To avoid double counting the same cell, we used at most one dataset from each rat. In a cluster plot, each dot represents the peak amplitude of a spike on two of the four tetrode channels. Spikes that were clustered to be from the same cell are plotted in the same color. Grey color represents spikes that were simultaneously recorded on the same channels, but were not part of any hand picked single-unit clusters. Each page contains plots of spikes from the same tetrode. The first 13 tetrodes are for CA1 pyramidal cells. The remaining 6 tetrodes are for CA3 pyramidal cells. On each page, the top six panels are in absolute amplitude scale (uV). The bottom six panels plot the same amplitudes under Hadamard transformation. A cell that fires complex spikes represented as an elongated cluster shape in absolute amplitude space takes a more compressed shape under Hadamard transformation.

CA1 unit	ISO	Rate during SWS (Hz)	Rate outside ripples (Hz)	Rate inside ripples (Hz)	Burst probability during SWS	Burst probability outside ripples	Burst probability inside ripples
r1d1t18c2	53.14	0.60	0.57	1.25	0.14	0.14	0.12
r1d2t11c2	38.88	0.09	0.09	0.23	0.14	0.16	0.06
r1d2t11c4	21.89	0.12	0.10	0.65	0.09	0.08	0.10
r1d2t15c7	40.81	0.14	0.09	1.18	0.42	0.36	0.54
r4d1t2c2	37.92	0.15	0.13	0.50	0.28	0.30	0.23
r4d1t2c7	148.37	0.21	0.17	0.95	0.28	0.27	0.31
r4d1t2c9	66.93	0.29	0.14	2.48	0.33	0.24	0.43
r4d1t3c2	58.64	0.14	0.13	0.33	0.30	0.31	0.25
r4d1t3c5	85.47	0.19	0.16	0.76	0.41	0.37	0.55
r4d1t7c1	28.72	0.03	0.03	0.03	0.32	0.31	0.40
r4d1t7c3	22.79	0.04	0.04	0.05	0.45	0.44	0.50
r4d1t17c3	57.55	0.14	0.09	0.83	0.43	0.42	0.45
r4d1t22c4	27.92	0.11	0.06	0.87	0.27	0.24	0.30
r4d1t23c2	23.54	0.06	0.05	0.31	0.27	0.29	0.24
r4d1t23c4	34.11	0.15	0.08	1.26	0.27	0.30	0.24
r4d1t23c5	36.48	0.24	0.16	1.35	0.48	0.49	0.46
r5d1t11c3	53.34	0.12	0.07	0.83	0.27	0.31	0.22
r5d1t11c4	234.18	0.19	0.11	1.53	0.44	0.35	0.59
r5d1t11c8	58.69	0.29	0.26	0.93	0.30	0.30	0.28
r5d1t14c1	44.39	0.11	0.08	0.74	0.18	0.16	0.21
r5d1t16c2	43.16	0.05	0.04	0.26	0.29	0.31	0.25
r5d1t16c4	74.94	0.13	0.07	1.15	0.36	0.45	0.29
r5d1t16c5	64.44	0.08	0.05	0.57	0.24	0.27	0.18
r5d1t16c9	81.03	0.11	0.08	0.59	0.18	0.15	0.23
r5d1t16c22	133.69	0.33	0.25	1.68	0.20	0.19	0.22
r5d1t18c2	28.59	0.15	0.11	0.79	0.34	0.31	0.42
r5d1t18c7	125.66	0.17	0.12	0.95	0.30	0.24	0.45
r5d1t18c10	69.82	0.26	0.16	1.92	0.37	0.32	0.46

Table 6.1: Statistics of hand picked CA1 pyramidal cells

CA3 unit	ISO	Rate during SWS (Hz)	Rate outside ripples (Hz)	Rate inside ripples (Hz)	Burst probability during SWS	Burst probability outside ripples	Burst probability inside ripples
r1d1t1c4	23.35	0.05	0.05	0.19	0.47	0.45	0.61
r1d1t1c6	27.55	0.08	0.08	0.13	0.22	0.22	0.25
r1d1t1c12	56.20	0.08	0.06	0.54	0.37	0.36	0.40
r1d1t3c2	35.70	0.03	0.02	0.03	0.01	0.01	0.00
r1d1t3c3	35.23	0.04	0.04	0.13	0.27	0.25	0.46
r1d1t3c4	154.19	0.08	0.08	0.08	0.15	0.14	0.56
r1d1t3c5	31.98	0.06	0.05	0.21	0.30	0.27	0.48
r1d1t3c6	186.67	0.11	0.11	0.14	0.22	0.22	0.39
r1d1t3c7	79.72	0.16	0.14	0.54	0.41	0.41	0.42
r1d1t3c8	30.69	0.12	0.12	0.12	0.11	0.10	0.25
r1d1t3c9	39.45	0.19	0.19	0.19	0.12	0.11	0.40
r1d1t22c4	94.46	0.05	0.05	0.21	0.14	0.14	0.16
r1d1t22c6	28.18	0.13	0.12	0.25	0.12	0.13	0.11
r1d1t22c8	75.76	0.18	0.18	0.26	0.09	0.10	0.06
r1d1t23c5	27.60	0.06	0.04	0.37	0.21	0.21	0.24
r1d1t24c1	17.87	0.05	0.04	0.23	0.40	0.39	0.45
r2d2t22c1	38.63	0.11	0.11	0.10	0.22	0.22	0.23
r2d2t22c2	37.31	0.08	0.07	0.10	0.46	0.47	0.41
r2d2t22c3	16.42	0.31	0.29	0.66	0.36	0.36	0.34
r2d2t22c6	48.60	0.43	0.41	0.77	0.32	0.32	0.31

Table 6.2: Statistics of hand picked CA3 pyramidal cells

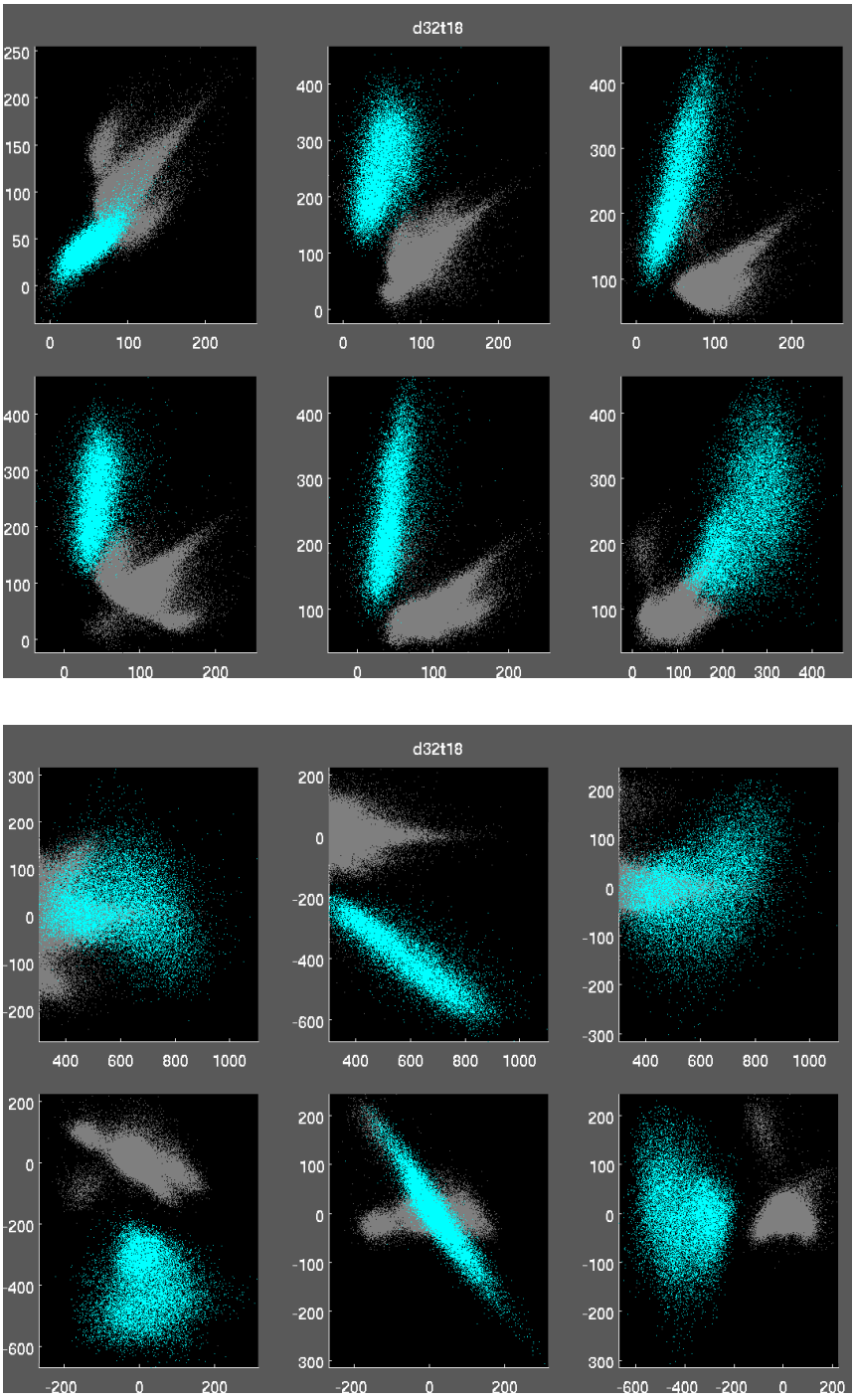

Figure 6.1: **Cluster plots: Rat 1, dataset 1, tetrode 18, CA1.** One unit was selected from this tetrode: r1d1t18c2 (cyan, rate in SWS = 0.6Hz, ISO = 53.14).

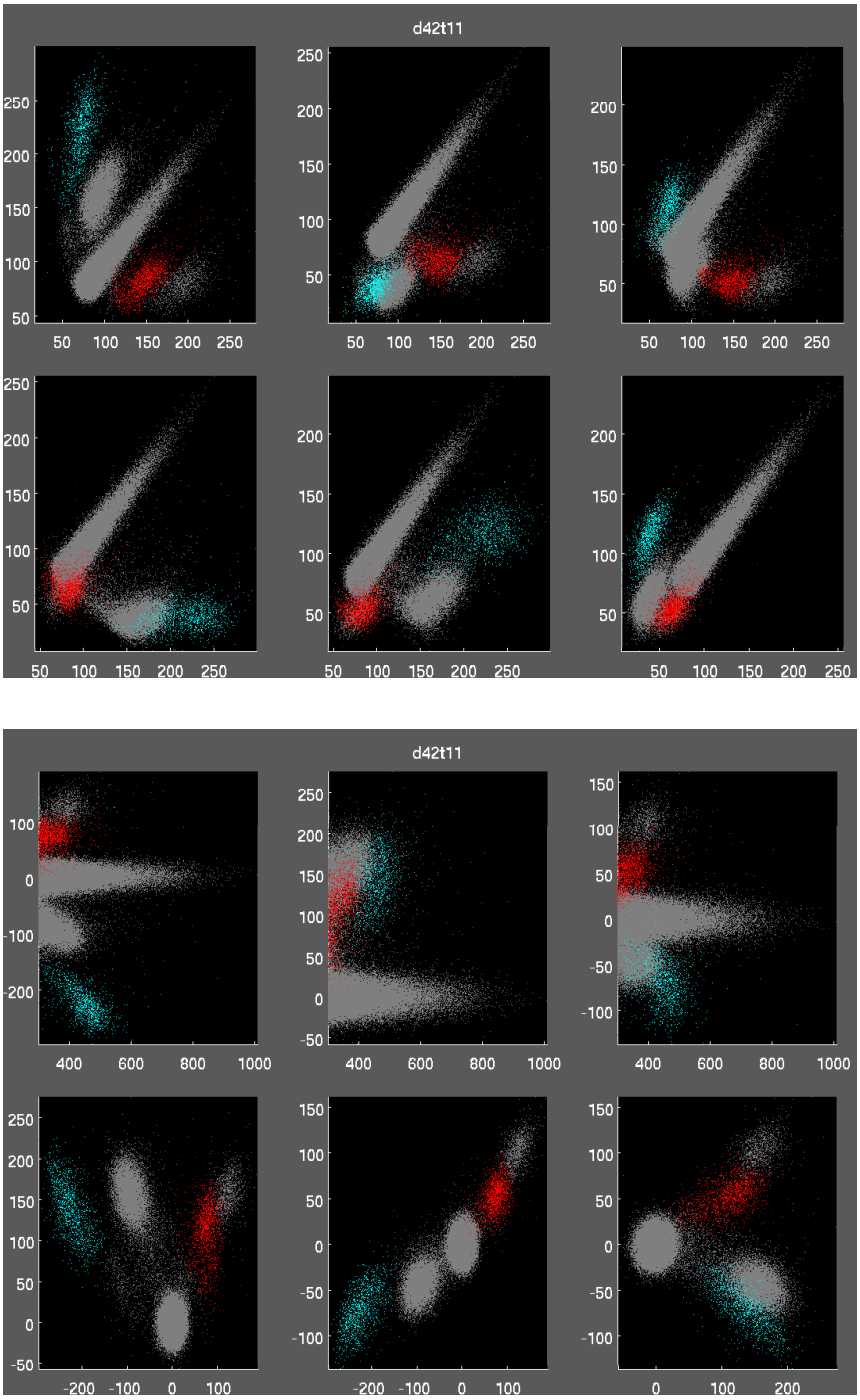

Figure 6.2: **Cluster plots: Rat 1, dataset 2, tetrode 11, CA1.** Two units were selected from this tetrode: r1d2t11c2 (cyan, rate in SWS = 0.09Hz, ISO = 38.88), r1d2t11c4 (red, rate in SWS = 0.12Hz, ISO = 21.89).

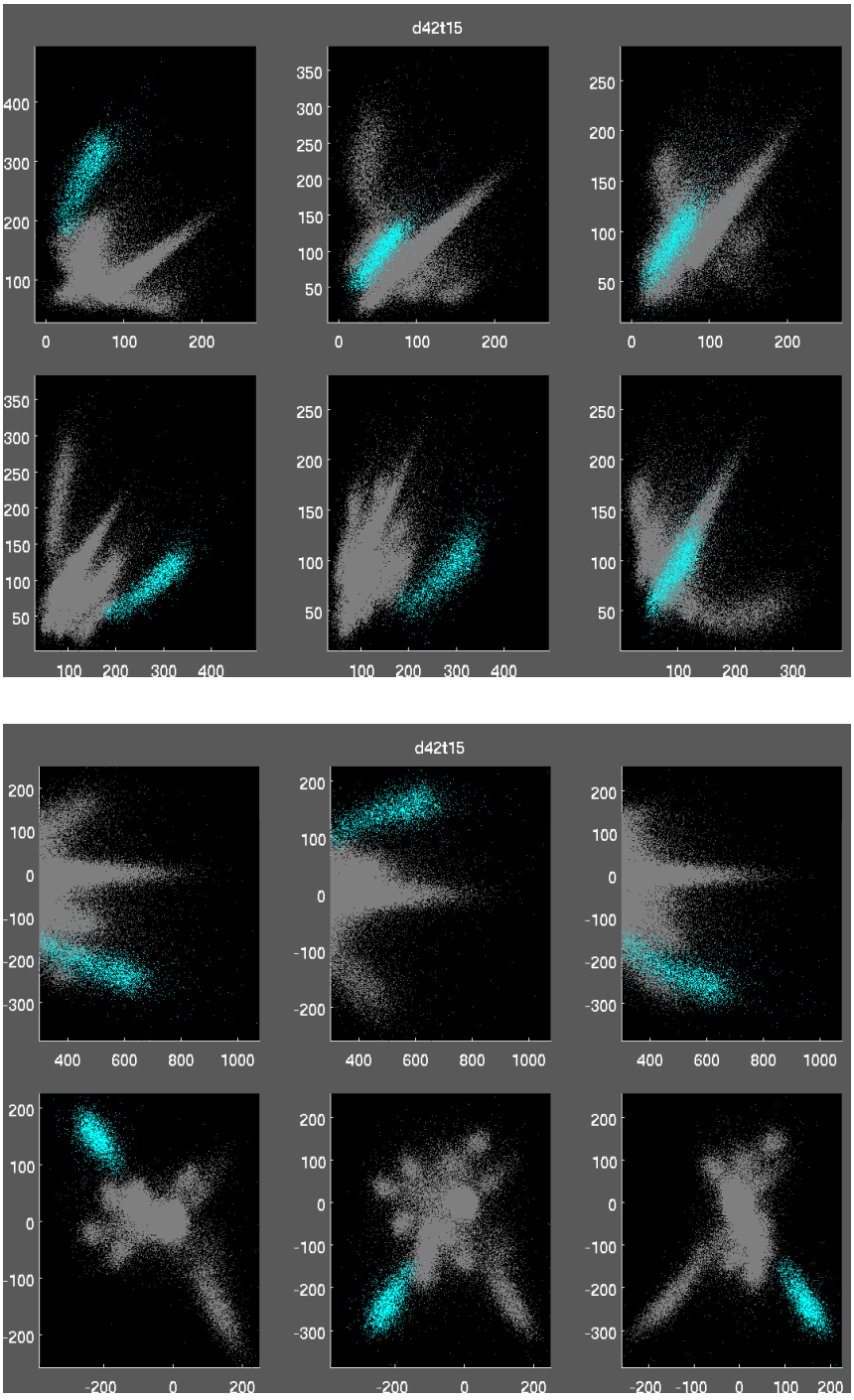

Figure 6.3: **Cluster plots: Rat 1, dataset 2, tetrode 15, CA1** One unit was selected from this tetrode: r1d2t15c7 (cyan, rate in SWS = 0.14Hz, ISO = 40.81).

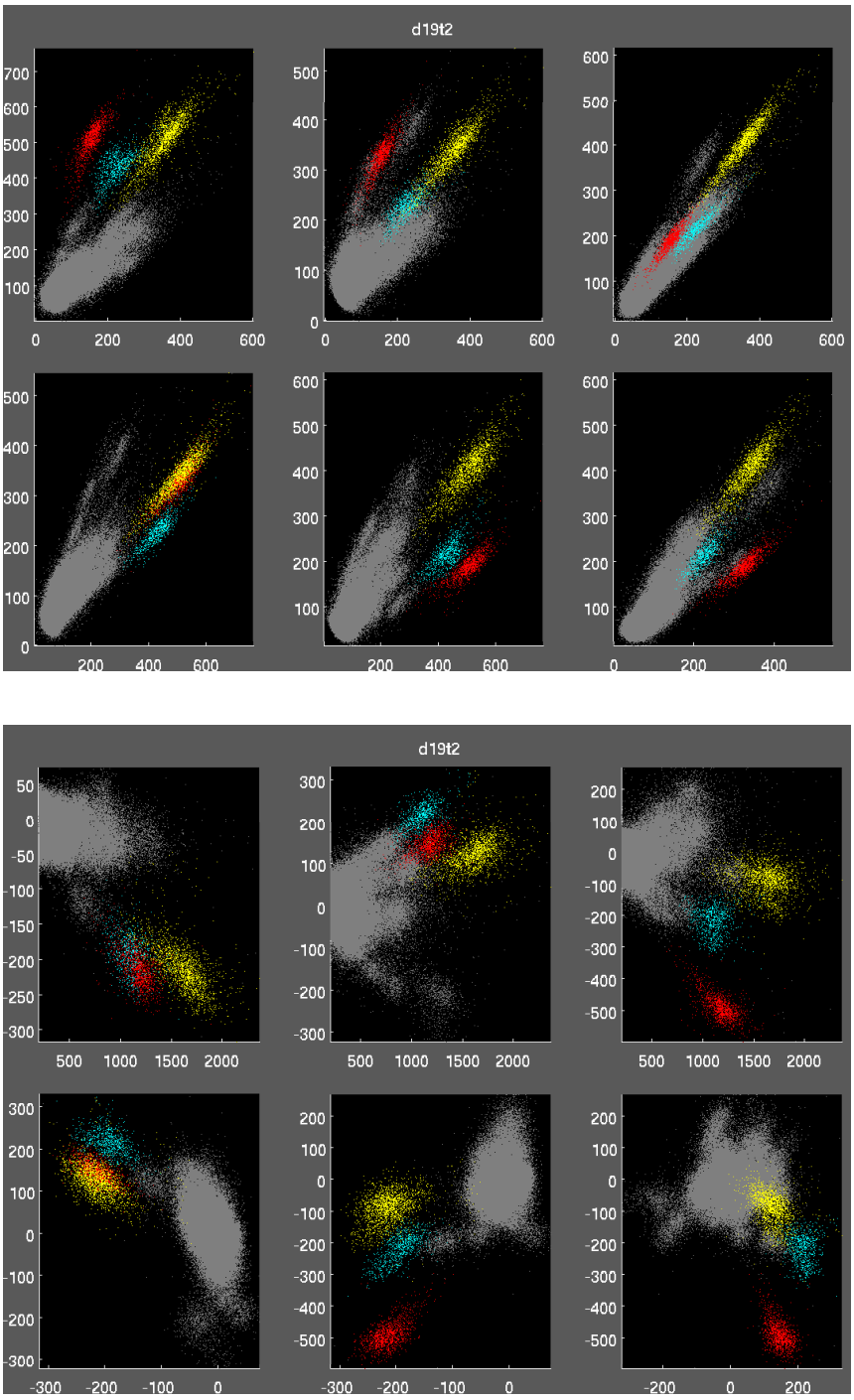

Figure 6.4: **Cluster plots: Rat 4, dataset 1, tetrode 2, CA1.** Three units were selected from this tetrode: r4d1t2c2 (cyan, rate in SWS = 0.15Hz, ISO = 37.92), r4d1t2c7 (red, rate in SWS = 0.21Hz, ISO = 148.37), r4d1t2c9 (yellow, rate in SWs = 0.29Hz, ISO = 66.93).

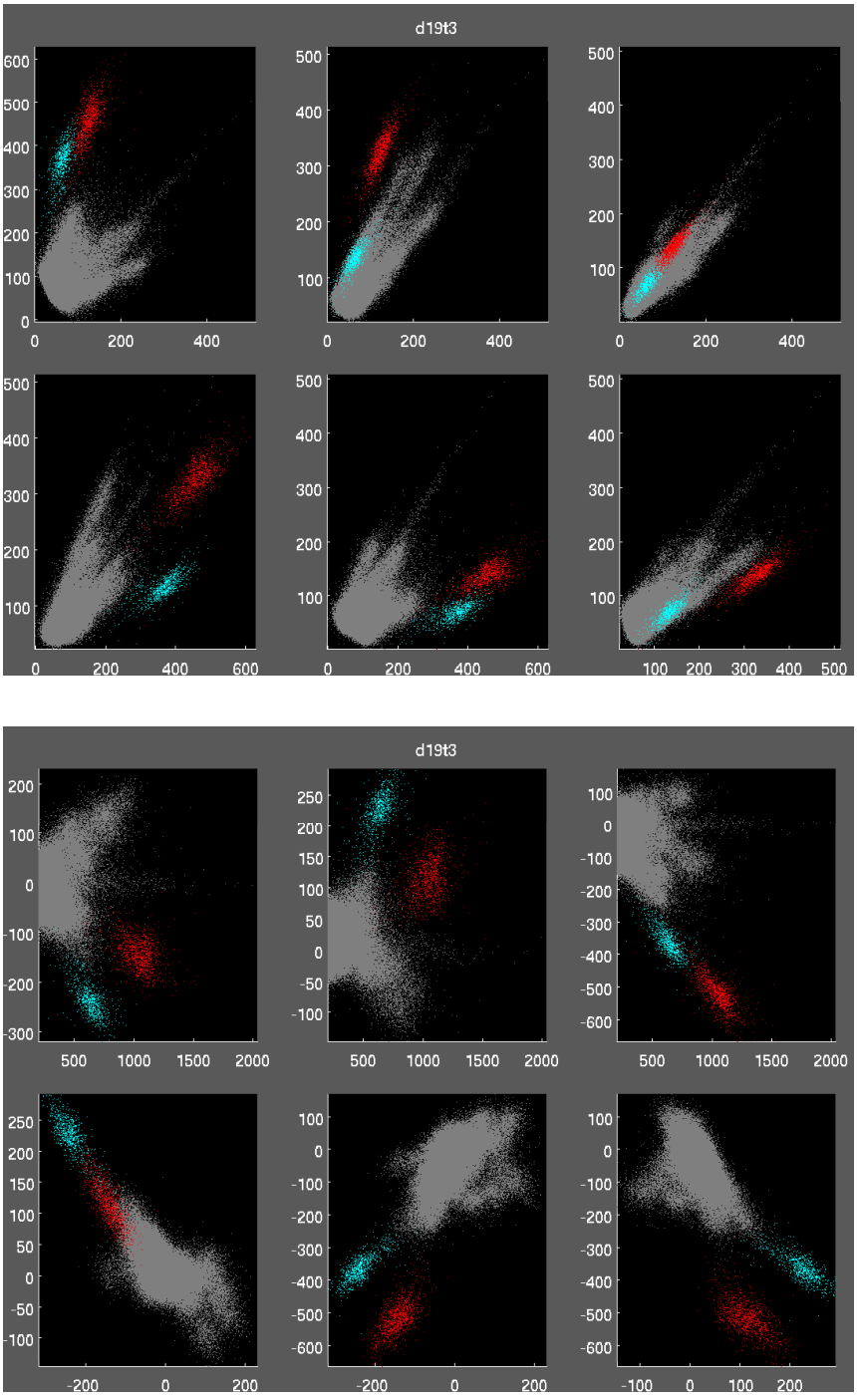

Figure 6.5: **Cluster plots: Rat 4, dataset 1, tetrode 3, CA1.** Two units were selected from this tetrode: r4d1t3c2 (cyan, rate in SWS = 0.14Hz, ISO = 58.64), r4d1t3c5 (red, rate in SWS = 0.19Hz, ISO = 85.47).

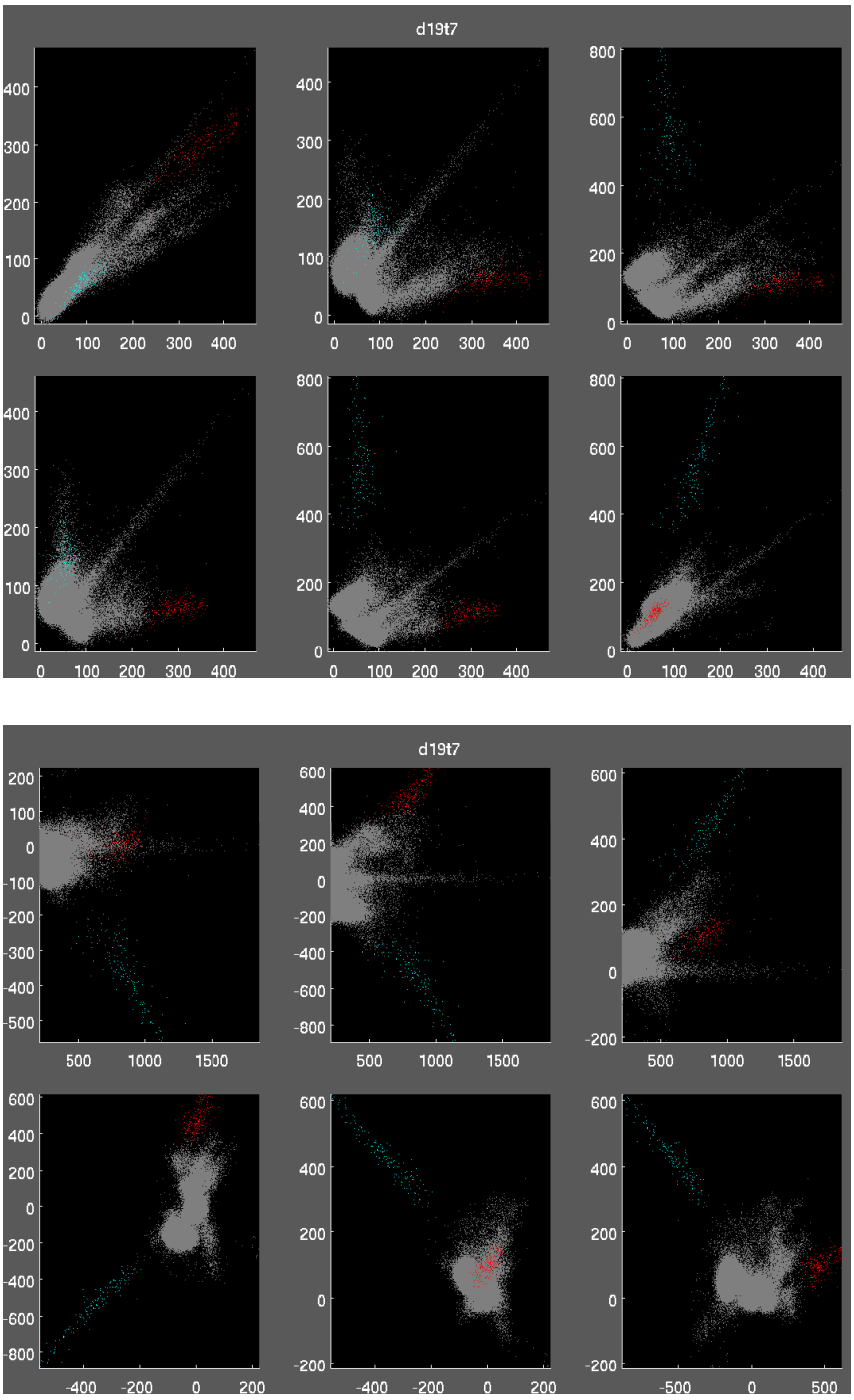

Figure 6.6: **Cluster plots: Rat 4, dataset 1, tetrode 7, CA1.** Two units were selected from this tetrode: r4d1t7c1 (cyan, rate in SWS = 0.03Hz, ISO = 28.72), r4d1t7c3 (red, rate in SWS = 0.04Hz, ISO = 22.79).

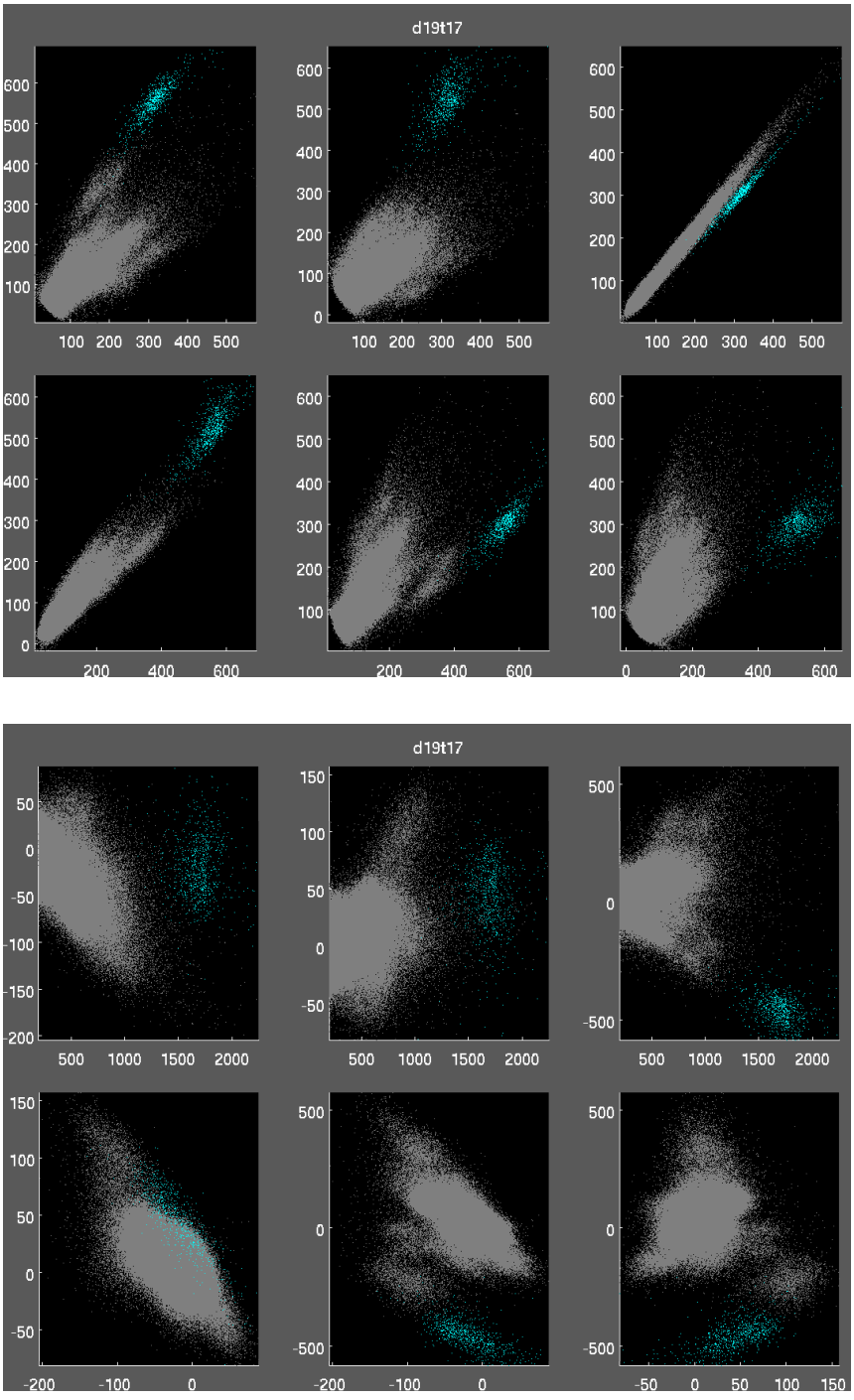

Figure 6.7: **Cluster plots: Rat 4, dataset 1, tetrode 17, CA1.** One unit was selected from this tetrode: r4d1t17c3 (cyan, rate in SWS = 0.14Hz, ISO = 57.55).

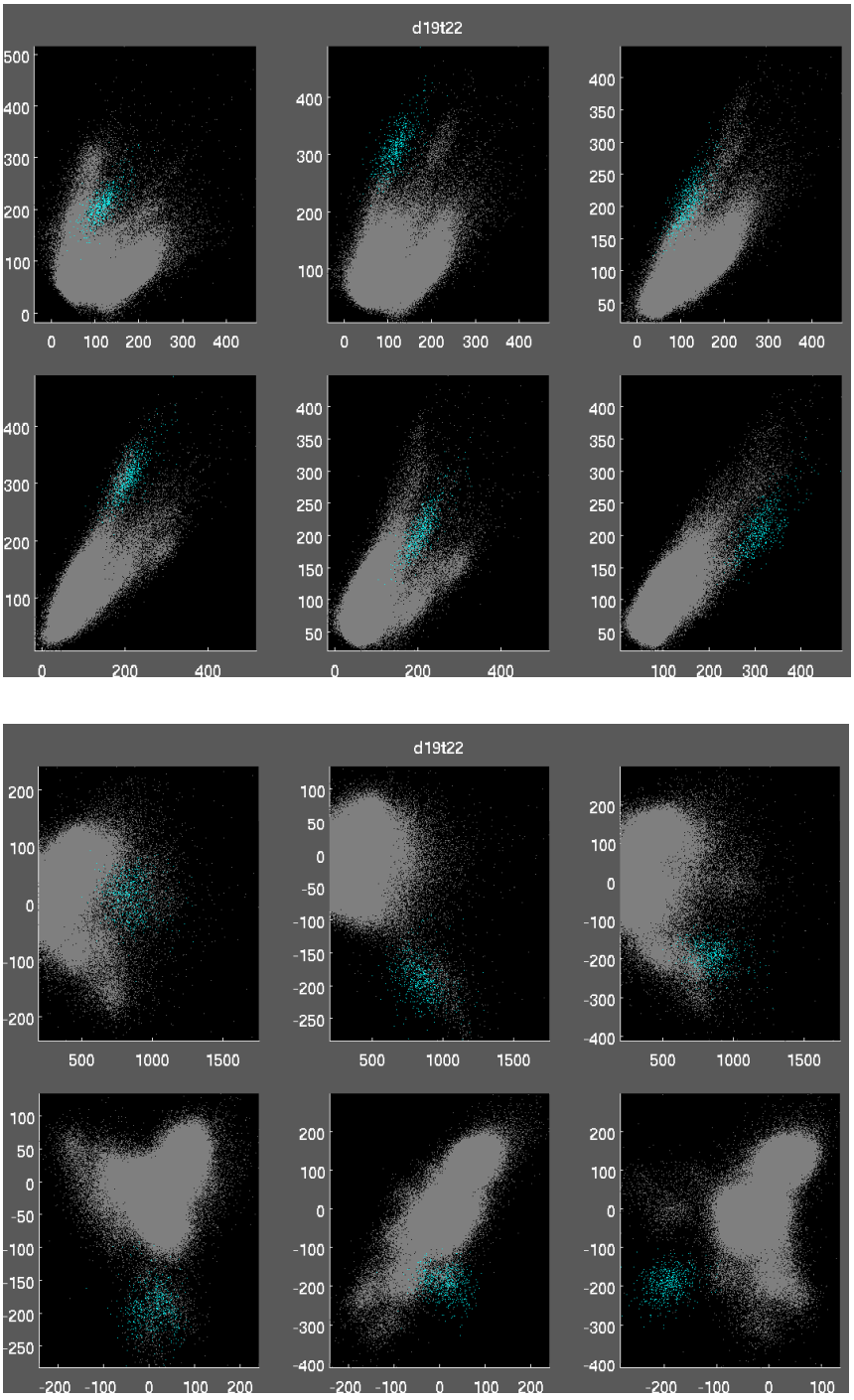

Figure 6.8: **Cluster plots: Rat 4, dataset 1, tetrode 22, CA1.** One unit was selected from this tetrode: r4d1t22c4 (cyan, rate in SWS = 0.11Hz, ISO = 27.92).

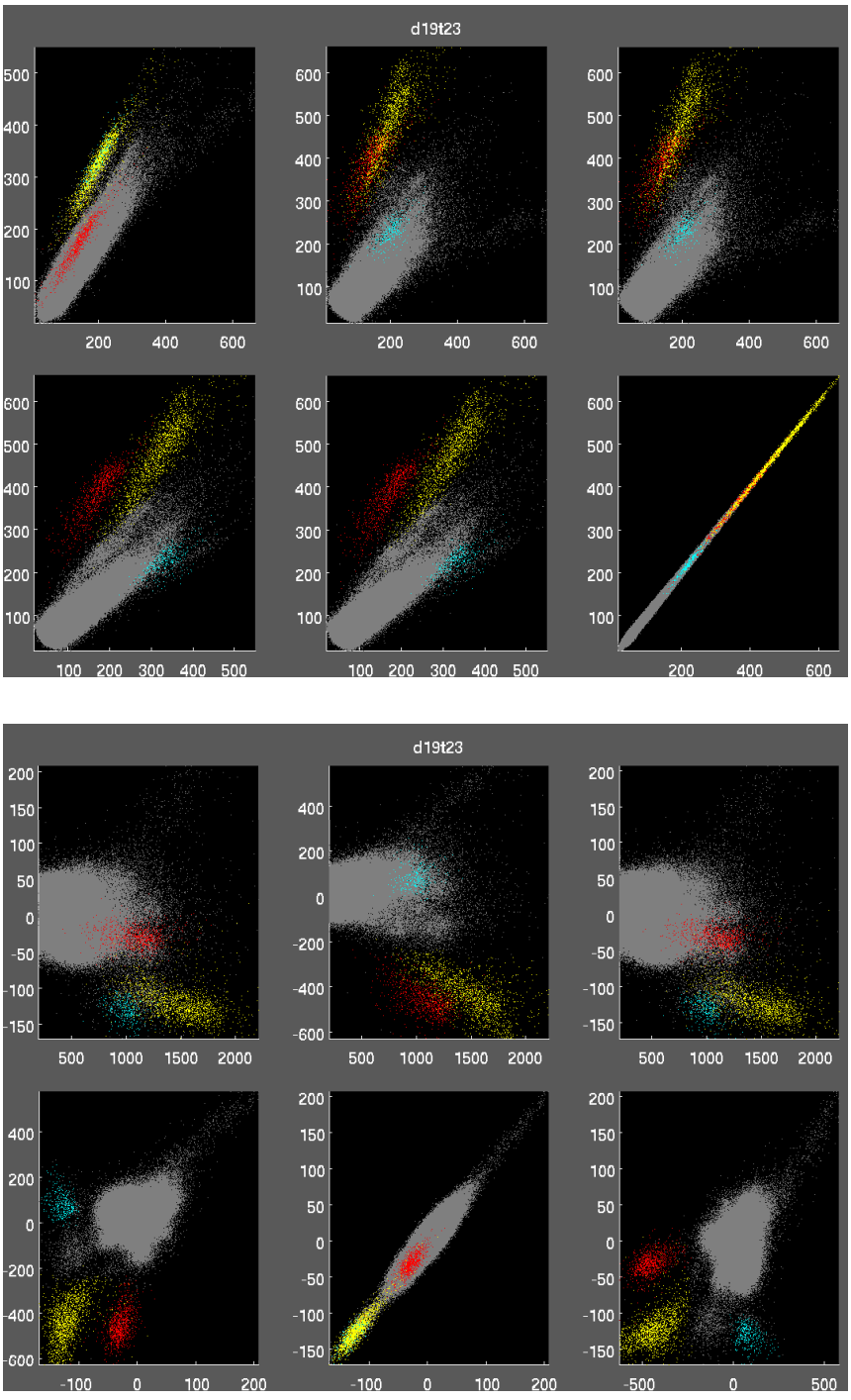

Figure 6.9: **Cluster plots: Rat 4, dataset 1, tetrode 23, CA1.** Three units were selected from this tetrode: r4d1t23c2 (cyan, rate in SWS = 0.06Hz, ISO = 23.54), r4d1t23c4 (red, rate in SWS = 0.15Hz, ISO = 34.11), r4d1t23c5 (yellow, rate in SWS = 0.24Hz, ISO = 36.48).

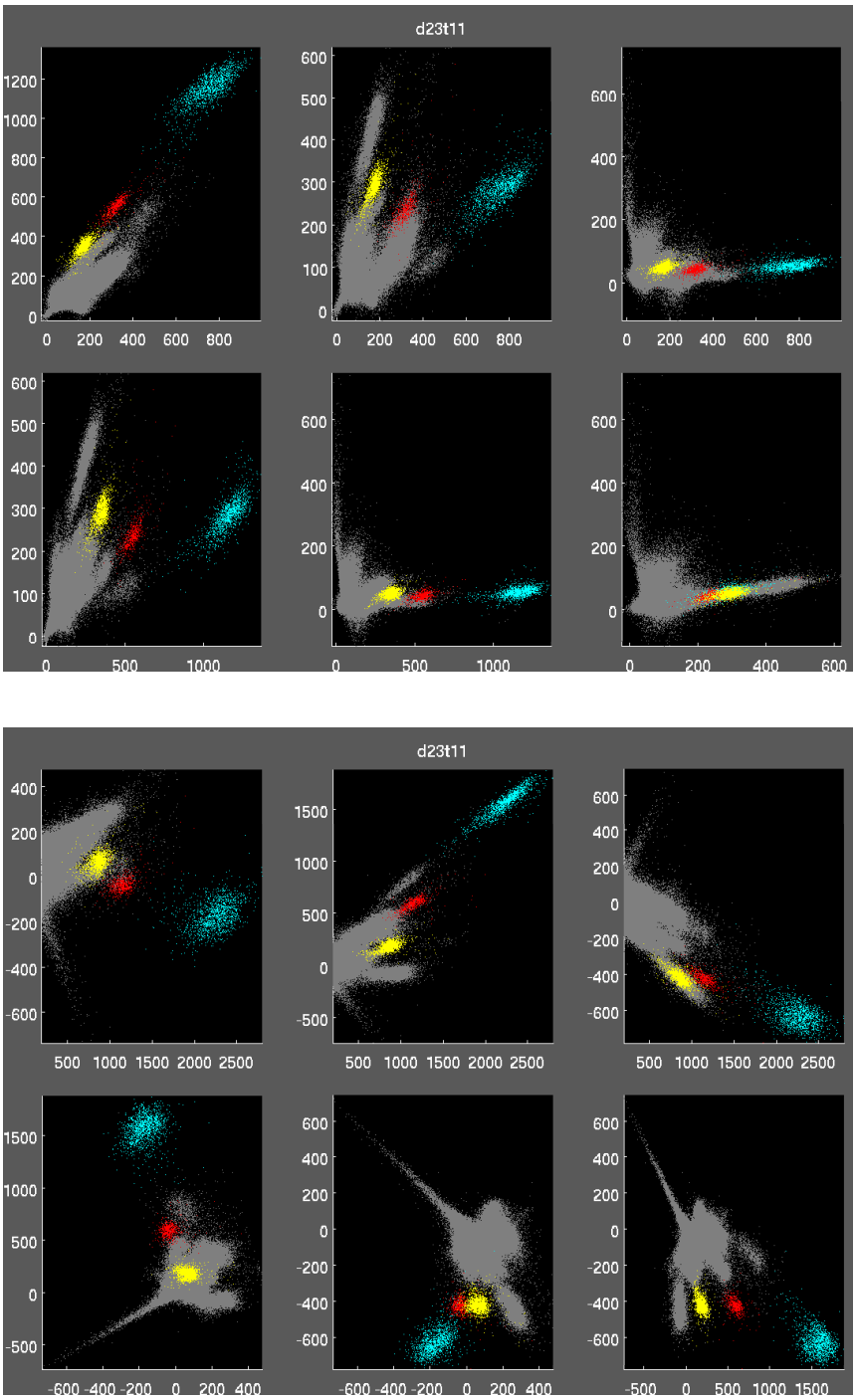

Figure 6.10: **Cluster plots: Rat 5, dataset 1, tetrode 11, CA1.** Three units were selected from this tetrode: r5d1t11c3 (cyan, rate in SWS = 0.12Hz, ISO = 53.34), r5d1t11c4 (red, rate in SWS = 0.19Hz, ISO = 234.18), r5d1t11c8 (yellow, rate in SWS = 0.29Hz, ISO = 58.69).

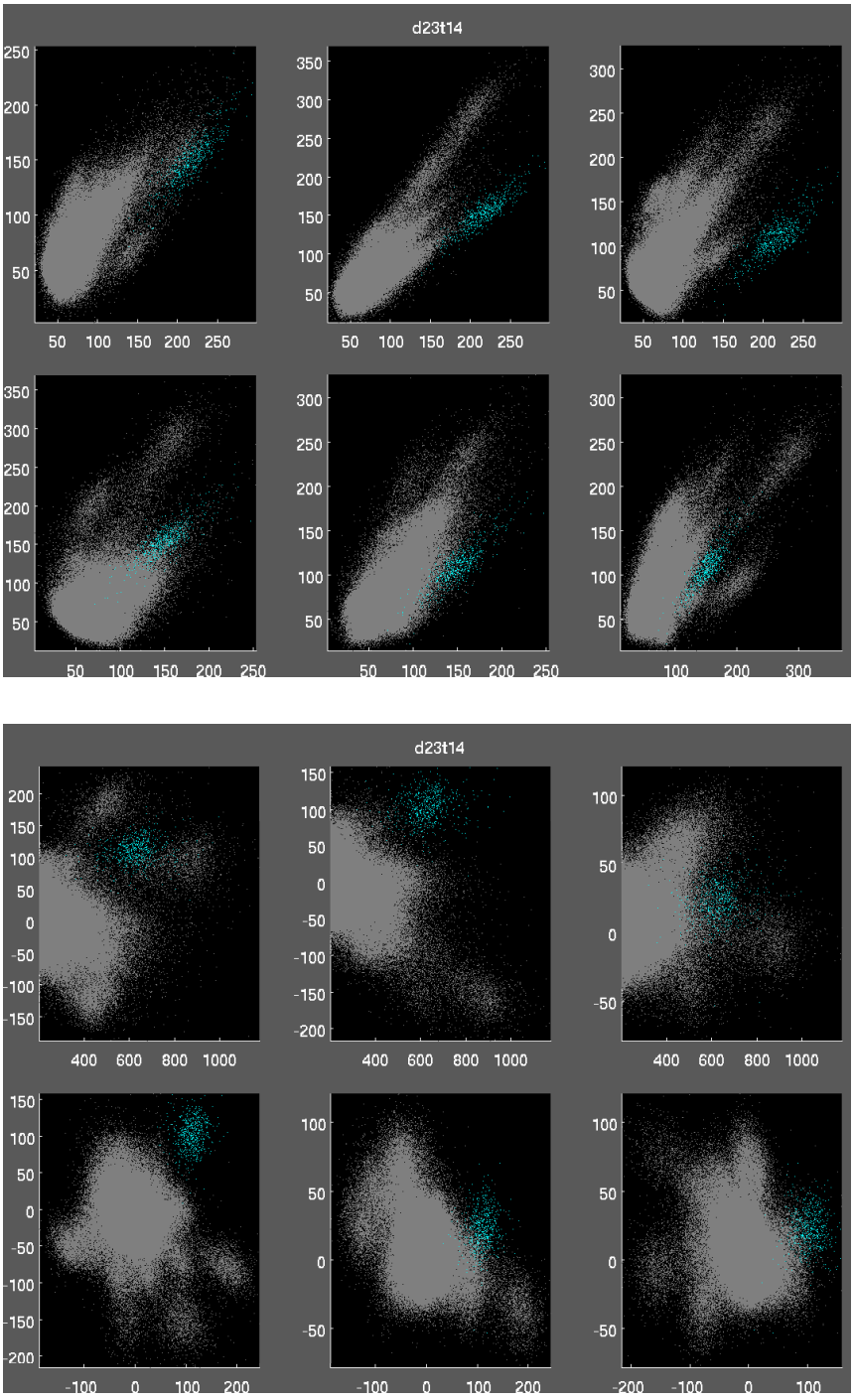

Figure 6.11: **Cluster plots: Rat 5, dataset 1, tetrode 14, CA1.** One unit was selected from this tetrode: r5d1t14c1 (cyan, rate in SWS = 0.11Hz, ISO = 44.39).

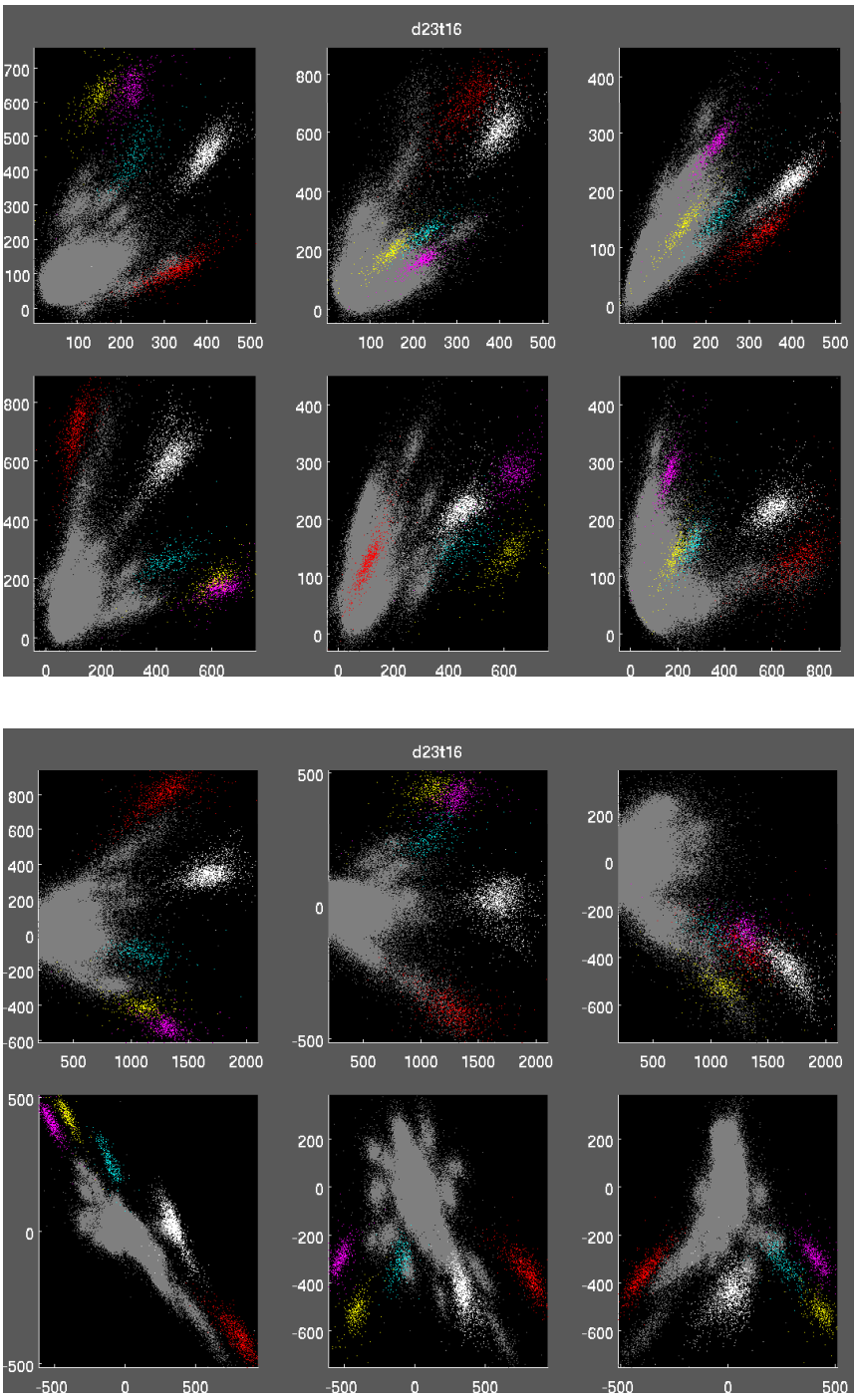

Figure 6.12: **Cluster plots: Rat 5, dataset 1, tetrode 16, CA1.** Five units were selected from this tetrode: r5d1t16c2 (cyan, rate in SWS = 0.05Hz, ISO = 43.16), r5d1t16c4 (red, rate in SWS = 0.13, ISo = 74.94), r5d1t16c5 (yellow, rate in SWS = 0.08Hz, ISO = 64.44), r5d1t16c9 (magenta, rate in SWS = 0.11, ISO = 81.03), r5d1t16c22 (white, rate in SWS = 0.33Hz, ISO = 133.69).

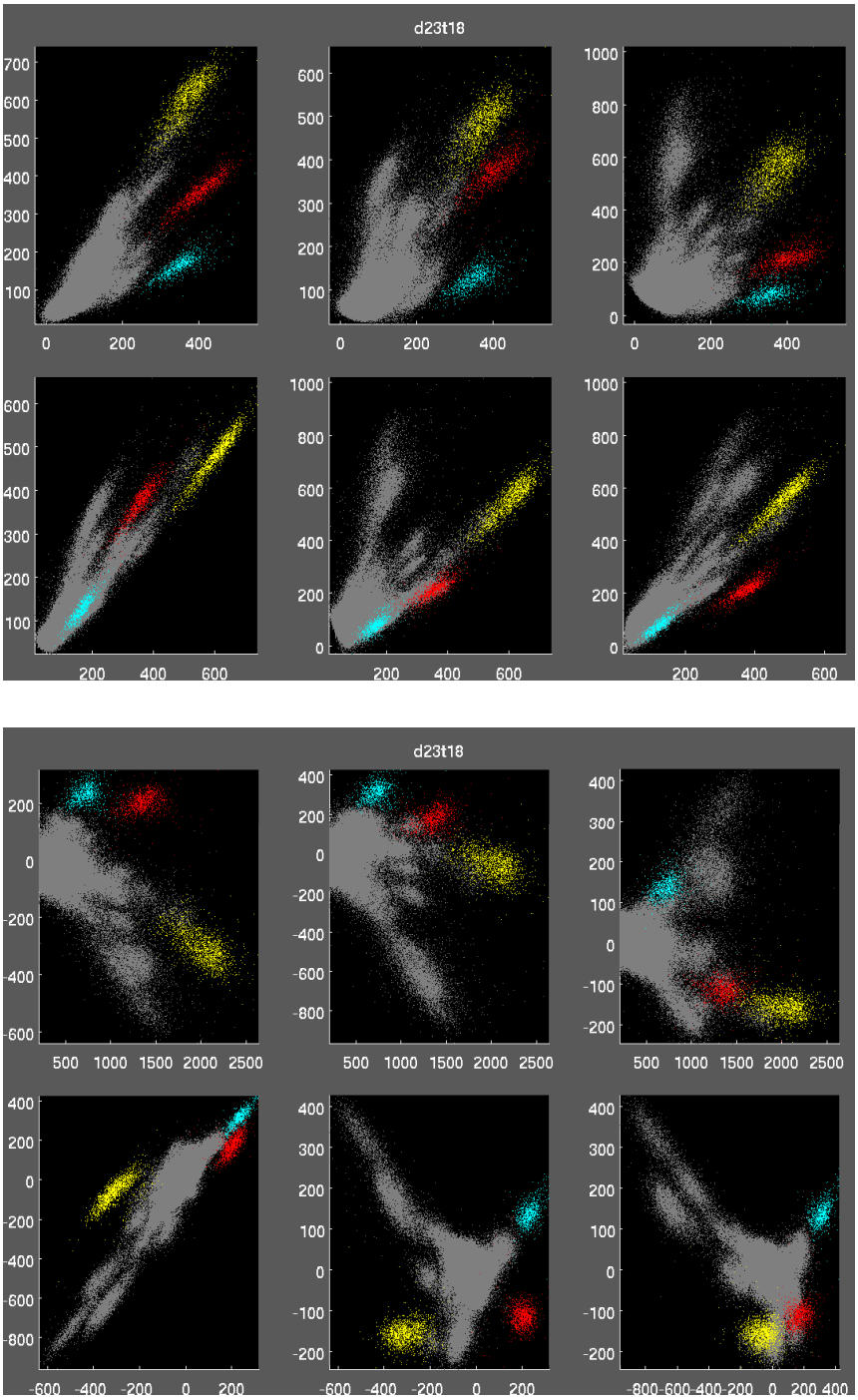

Figure 6.13: **Cluster plots: Rat 5, dataset 1, tetrode 18, CA1.** Three units were selected from this tetrode: r5d1t18c2 (cyan, rate in SWS = 0.15Hz, ISO = 28.59), r5d1t18c7 (red, rate in SWS = 0.17Hz, ISO = 125.66), r5d1t18c10 (yellow, rate in SWS = 0.26Hz, ISO = 69.82).

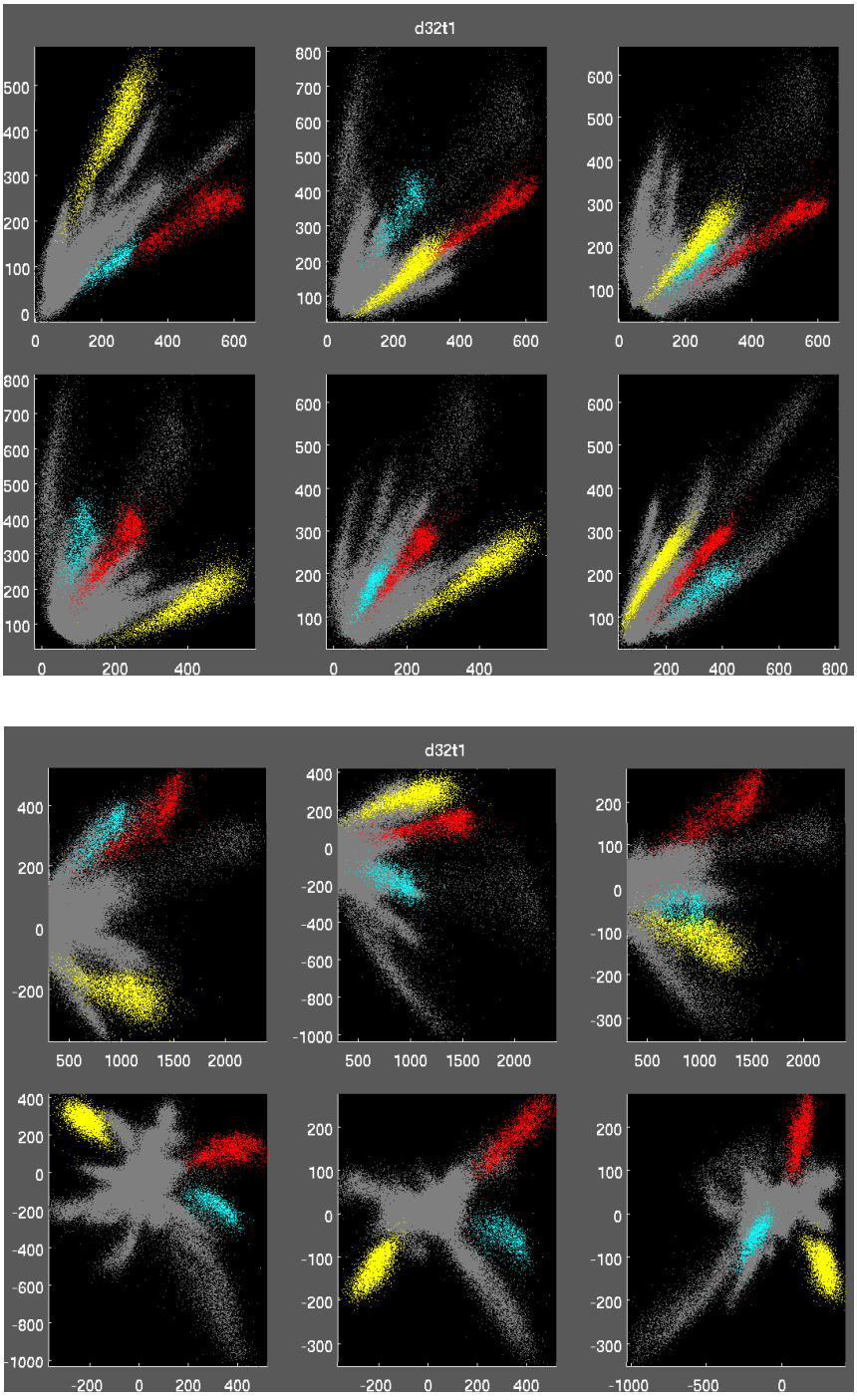

Figure 6.14: **Cluster plots: Rat 1, dataset 1, tetrode 1, CA3.** Three units were selected from this tetrode: r1d1t1c4 (cyan, rate in SWS = 0.05Hz, ISO = 23.35), r1d1t1c6 (red, rate in SWS = 0.08Hz, ISO = 27.55), r1d1t1c12 (yellow, rate in SWS = 0.08Hz, ISO = 56.20).

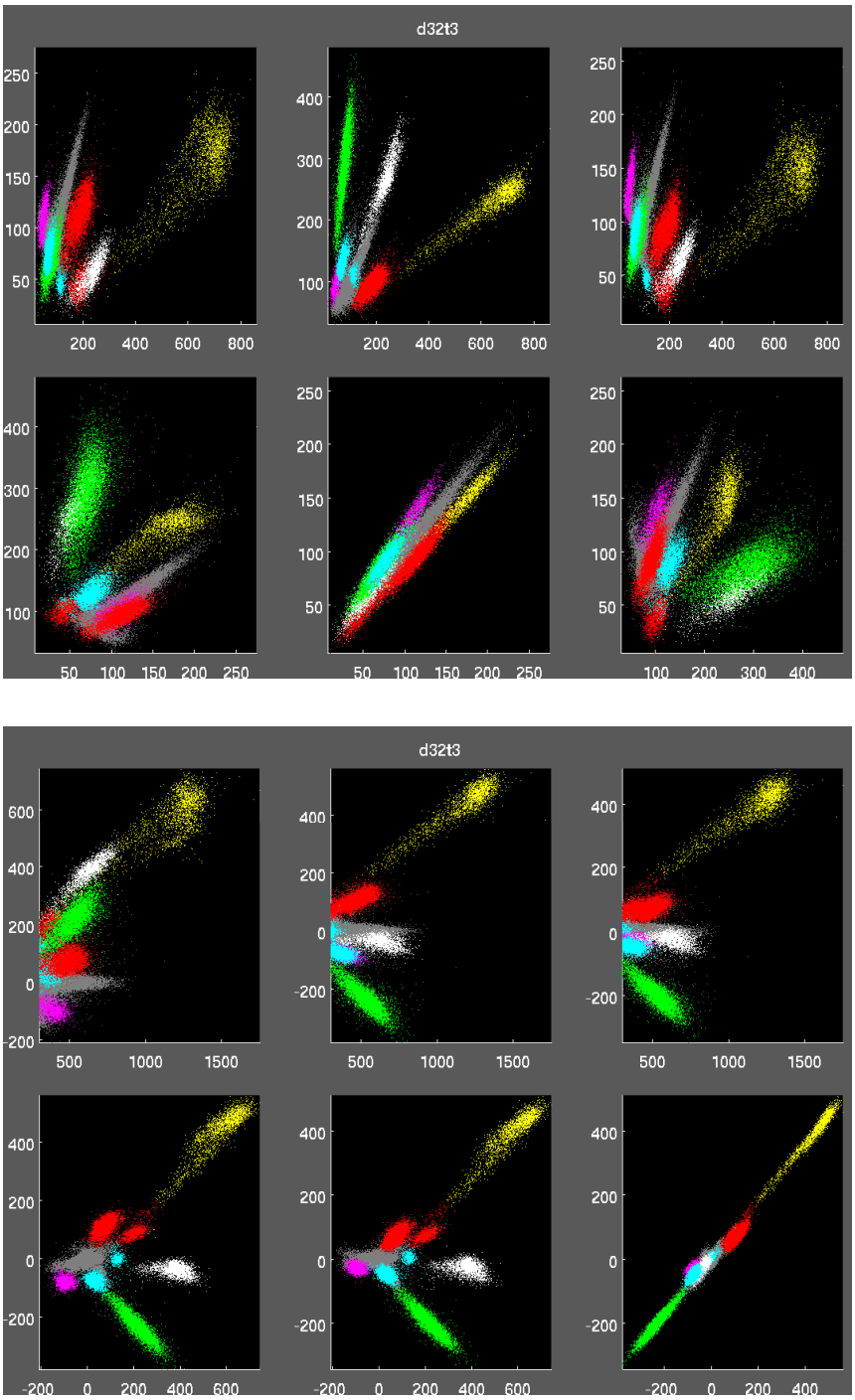

Figure 6.15: **Cluster plots: Rat 1, dataset 1, tetrode 3, CA3.** Eight units were selected from this tetrode: r1d1t3c2 (cyan, rate in SWS = 0.03Hz, ISO = 35.70), r1d1t3c3 (red, rate in SWS = 0.04Hz, ISO = 35.23), r1d1t3c4 (yellow, rate in SWS = 0.08Hz, ISO = 154.19), r1d1t3c5 (magenta, rate in SWS = 0.06Hz, ISO = 31.98), r1d1t3c6 (white, rate in SWS = 0.11Hz, ISO = 186.67), r1d1t3c7 (green, rate in SWS = 0.16Hz, ISO = 79.72), r1d1t3c8 (cyan2, rate in SWS = 0.12Hz, ISO = 30.69), r1d1t3c9 (red2, rate in SWS = 0.19Hz, ISO = 39.45).

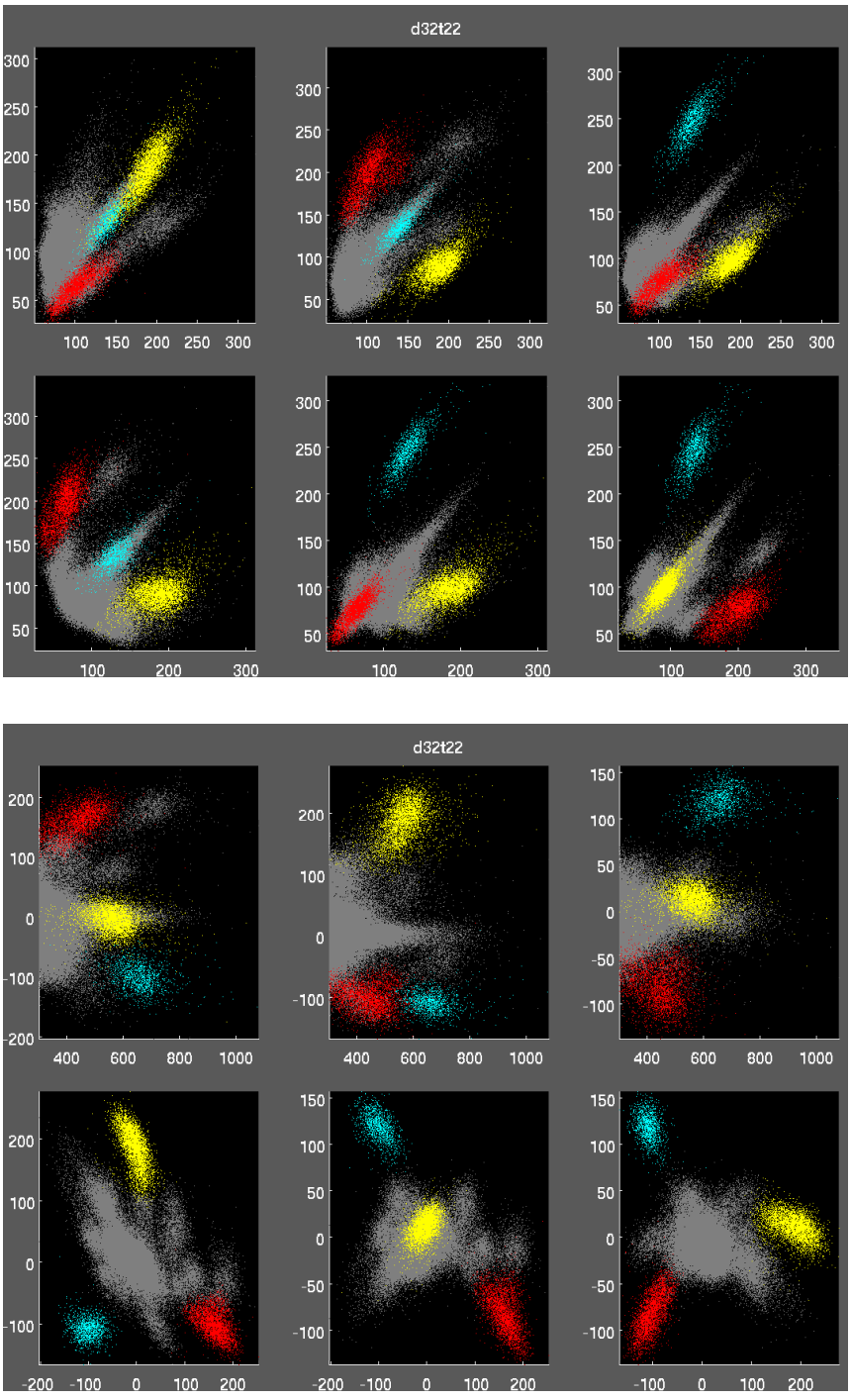

Figure 6.16: **Cluster plots: Rat 1, dataset 1, tetrode 22, CA3.** Three units were selected from this tetrode: r1d1t22c4 (cyan, rate in SWS = 0.05Hz, ISO = 94.46), r1d1t22c6 (red, rate in SWS = 0.13Hz, ISO = 28.18), r1d1t22c8 (yellow, rate in SWS = 0.18Hz, ISO = 75.76).

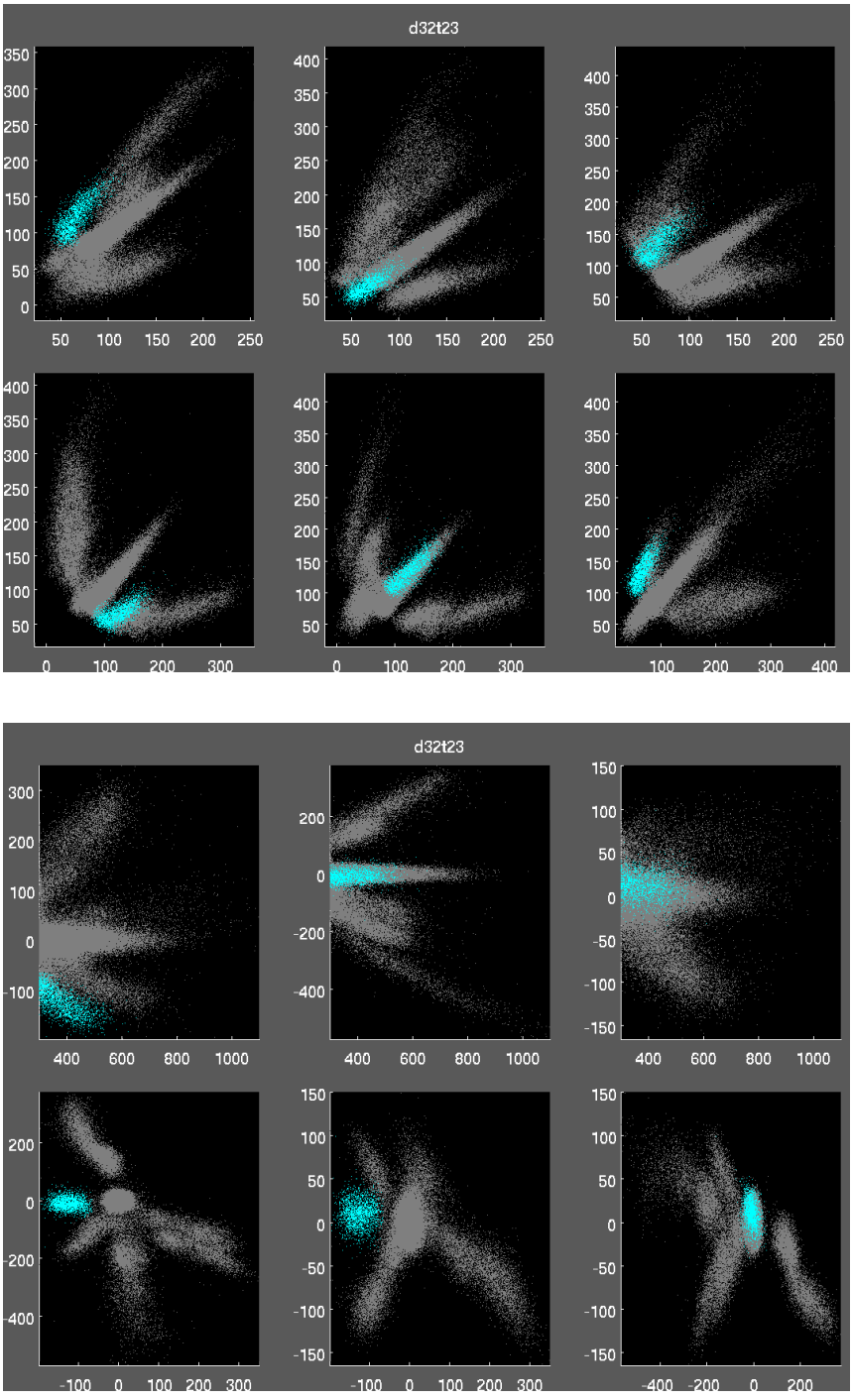

Figure 6.17: **Cluster plots: Rat 1, dataset 1, tetrode 23, CA3.** One unit was selected from this tetrode: r1d1t23c5 (cyan, rate in SWS = 0.06Hz, ISO = 27.60).

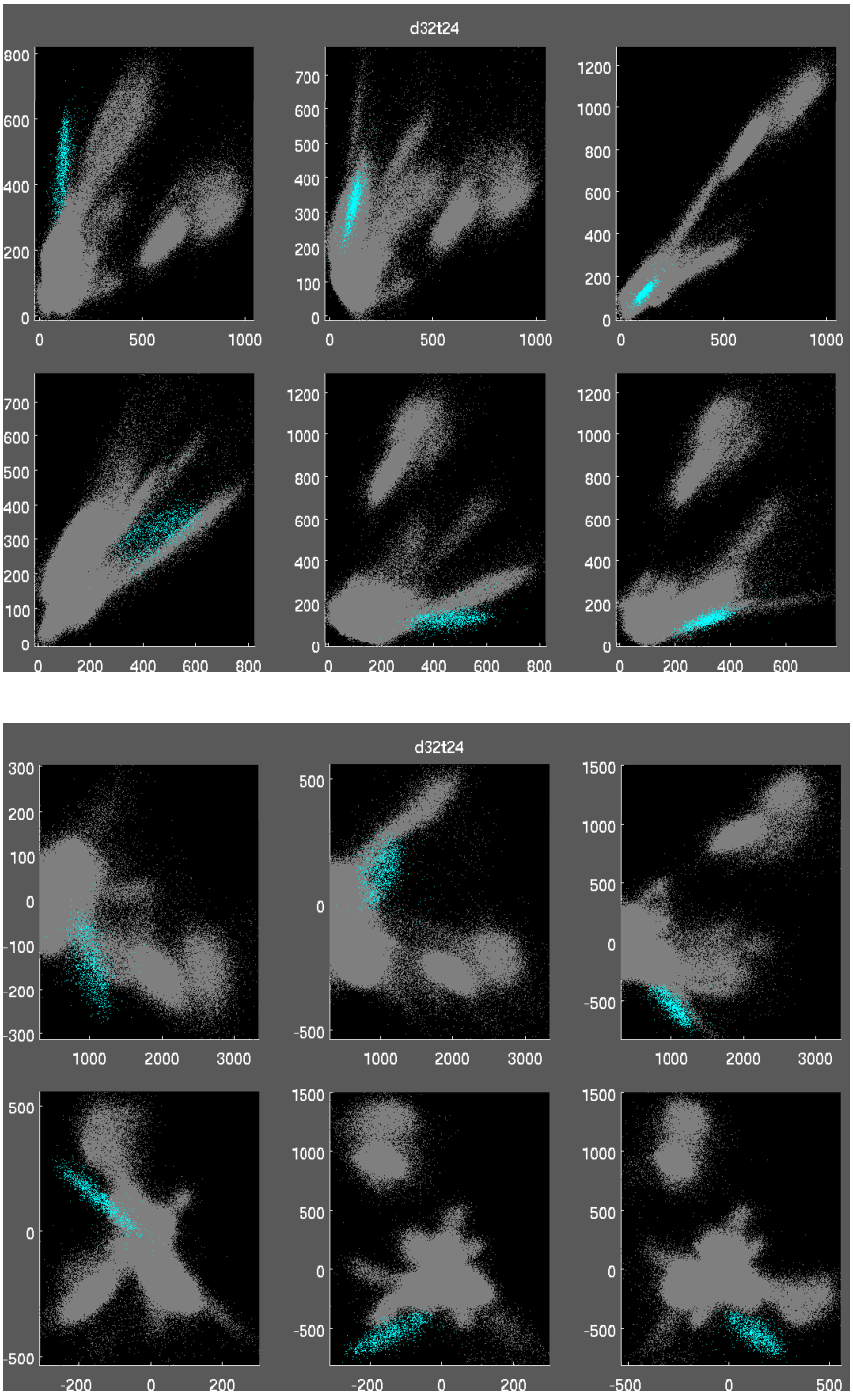

Figure 6.18: **Cluster plots: Rat 1, dataset 1, tetrode 24, CA3.** One unit was selected from this tetrode: r1d1t24c1 (cyan, rate in SWS = 0.05Hz, ISO = 17.87).

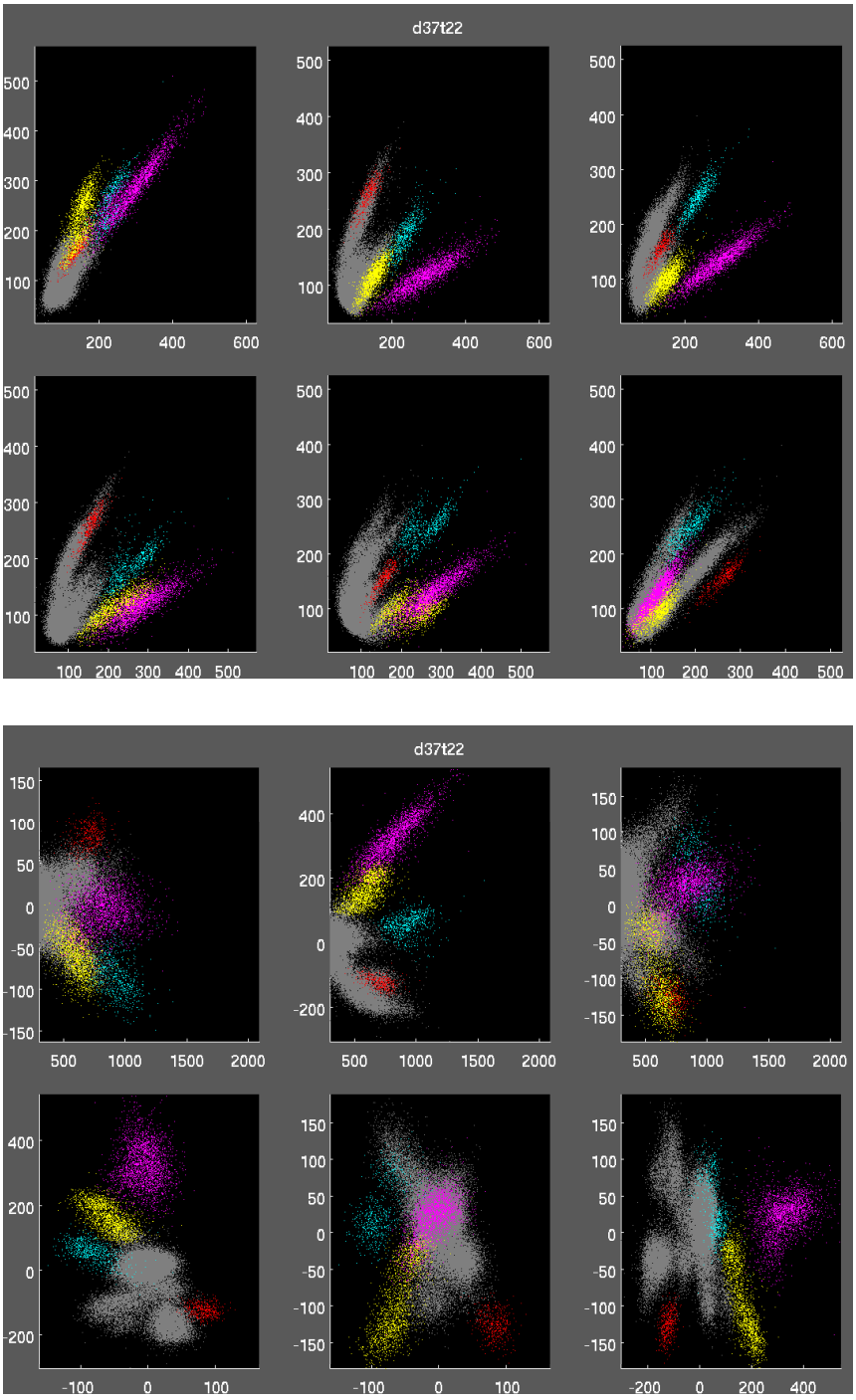

Figure 6.19: **Cluster plots: Rat 2, dataset 1, tetrode 22, CA3.** Four units were selected from this tetrode: r2d2t22c1 (cyan, rate in SWS = 0.11Hz, ISO = 38.63), r2d2t22c2 (red, rate in SWS = 0.08Hz, ISO = 37.31), r2d2t22c3 (yellow, rate in SWS = 0.31Hz, ISO = 16.42), r2d2t22c6 (magenta, rate in SWS = 0.43Hz, ISO = 48.60).

Bibliography

[1] Squire L.R. Memory and the hippocampus: A synthesis from findings with rats, monkeys, and humans. *Psychological Review*, 99(2):195–231, 1992.

[2] Squire L.R. and Alvarez P. Retrograde amnesia and memory consolidation: a neurobiological perspective. *Curr. Opin. Neurobiol.*, 5(2):169–177, 1995.

[3] Scoville W. B. and Milner B. Loss of recent memory after bilateral hippocampal lesions. *J. Neurol. Neurosurg. Psychiatry*, 20:11–21, 1957.

[4] Sutherland R.W. and McDonald R.J. Hippocampus, amygdala, and memory deficits in rats. *Behavioral Brain Research*, 37:57–79, 1990.

[5] Eichenbaum H., Fagan A., and Cohen N.J. Normal olfactory discrimination learning set and facilitation of reversal learning after medial-temporal damage in rats: Implication for an account of preserved learning abilities in amnesia. *J. Neurosci.*, 6:1876–1884, 1986.

[6] Aggleton J.P., Hunt P.R., and Rawlins J.N.P. The effects of hippocampal lesions upon spatial and non-spatial tests of working memory. *Behavioral Brain Research*, 19:133–146, 1986.

[7] Takehara K., Kawahara S., and Kirino Y. Time-dependent reorganization of the brain components underlying memory retention in trace eyeblink conditioning. *J. Neurosci.*, 23(30):9897–9905, 2003.

[8] Buzsáki G. Two-stage model of memory trace formation: a role for "noisy" brain states. *Neuroscience*, 31:551–570, 1989.

[9] Paxinos G. *The Rat Nervous System*. Academic Press, 2nd edition edition, 1994.

[10] Andersen P., Morris R., Amaral D., Bliss T., and O'keefe J. *The Hippocampus Book*. Oxford University Press, USA, 1st edition edition, 2006.

[11] Hopfield J.J. Neural networks and physical systems with emergent collective computational abilities. *PNAS*, 79:2554–2558, 1982.

[12] Ishizuka N., Weber J., and Amaral D. Organization of intrahippocampal projections originating from CA3 pyramidal cells in the rat. *J. Comp. Neurol.*, 295:580–623, 1990.

[13] Debanne D., Gahwiler B.H., and Thompson S.M. Long-term synaptic plasticity between pairs of individual ca3 pyramidal cells in rat hippocampal slice cultures. *J. Physiol.*, 507:237–247, 1998.

[14] Bennett M.R., Gibson W.G., and Robinson J. Dynamics of the ca3 pyramidal neuron autoassociative memory network in the hippocampus. *Philos. Trans. R. Soc. Lond. B Biol. Sci.*, 343:167–187, 1994.

[15] Wieber S.P., Stäubli U.V., and Ambros-Ingerson J. Short-term reverberant memory model of hippocampal field ca3. *Hippocampus*, 7:656–665, 1997.

[16] Sommer F.T. and Wennekers T. Associative memroy in networks of spiking neurons. *Neural Networks*, 14:825–834, 2001.

[17] Crick F. and Mitchison G. The function of dream sleep. *Nature*, 304:111–114, 1983.

[18] Siegel J.M. The REM sleep-memory consolidation hypothesis. *Science*, 294:1058–1063, 2001.

[19] R. Stickgold, J.A. Hobson, R. Fosse, and M. Fosse. Sleep, learning, and dreams: Off-line memory reprocessing. *Science*, 294:1052–1057, 2001.

[20] Wilson M. Hippocampal memory formation, plasticity, and the role of sleep. *Neurobio. of Learning and Memory*, 78:565–9, 2002.

[21] Walker M. and Stickgold R. Sleep-dependent learning and memory consolidation. *Neuron*, 44:121–133, 2004.

[22] Nakazawa K., Sun L.D., Quirk M.C., Rondi-Reig L., Wilson M.A., and Tonegawa S. Hippocampal ca3 nmda receptors are crucial for memory acquisition of one-time experience. *Neuron*, 38:305–315, 2003.

[23] Nakashiba T., Buhl D.L., McHugh T.J., and Tonegawa S. Hippocampal ca3 output is crucial for ripple-associated reactivation and consolidation of memory. *Neuron*, 62:781–787, 2009.

[24] Swanson L. and Cowan W.M. Hippocampus-hypothalamic connections: Origin in subicular cortex, not ammon's horn. *Science*, 25:303–304, 1975.

[25] Swanson L.W. and Cowan W.M. An autoradiographic study of the organization of the efferent connections of the hippocampal formation in the rat. *J. Comp. Neurol.*, 172:49–84, 1977.

[26] Tamamaki N., Watanabe K., and Nojyo Y. A whole image of the hippocampal pyramidal neuron revealed by intracellular pressure-injection of horseradish peroxidase. *Brain Res.*, 307:336–40, 1984.

[27] Tamamaki N., Abe K., and Nojyo Y. Three-dimensional analysis of the whole axonal arbors originating from single ca2 pyramidal neurons in the rat hippocampus with the aid of a computer graphic technique. *Brain Res.*, 452:255–72, 1988.

[28] Amaral D.G., Dolorfo C., and Alvarez-Royo P. Organization of ca1 projections to the subiculum: A pha-l analysis in the rat. *Hippocampus*, 1:415–436, 1991.

[29] Van Groen T. and Wyss J.M. Extrinsic projections from area CA1 of the rat hippocampus: olfactory, cortical, subcortical, and bilateral hippocampal formation projections. *J. Comp. Neurol.*, 302:515–528, 1990.

[30] Thierry A.M., Gioanni Y., and Dégénétais E. Hippocampo-prefrontal cortex pathway: anatomical and electrophysiological characteristics. *Hippocampus*, 10:411–419, 2000.

[31] Laroche S., Davis S., and Jay T.M. Plasticity at hippocampal to prefrontal cortex synapses: dual roles in working memory and consolidation. *Hippocampus*, 10:438–446, 2000.

[32] Sirota A., Csicsvári J., Buhl D., and Buzsáki G. Communication between neocortex and hippocampus during sleep in rodents. *PNAS*, 100:2065–2069, 2003.

[33] Buzsáki G. Hippocampal sharp waves: Their origin and significance. *Brain Res.*, 398:242–252, 1986.

[34] Chrobak J.J. and Buzsáki G. High-frequency oscillations in the output networks of the hippocampal-entorhinal axis of the freely behaving rat. *J. Neurosci.*, 16:3056–3066, 1996.

[35] Csicsvari J., Hirase H., Mamiya A., and Buzsáki G. Ensemble patterns of hippcampal CA3-CA1 neurons during sharp wave-associated population events. *Neuron*, 28:585–594, 2000.

[36] Buzsaki G., Horvath Z., Urioste R., Hetke J., and Wise K. High-frequency network oscillation in the hippocampus. *Science*, 256:1025, 1992.

[37] Ylinen A., Bragin A., Nadasdy Z., Jando G., Szabo I., Sik A., and Buzsáki G. Sharp wave associated high frequency oscillation (200 Hz) in the intact hippocampus: network and intracellular mechanisms. *J. Neurosci.*, 15:30–46, 1995.

[38] Wierzynski C.M., Lubenov E.V., Gu M., and Siapas A.G. State-dependent spike-timing relationships between hippocampal and prefrontal circuits during sleep. *Neuron*, 61:587–596, 2009.

[39] Ranck J.B.J. Studies on single neurons in dorsal hippocampal formation and septum in unrestrained rats. i. behavioral correlates and firing repertoires. *Exp. Neurol.*, 41:461–531, 1973.

[40] Sneider J.T., Chrobak J.J., Quirk M.C., Oler J.A., and Markus E.J. Differential behavioral state-dependence in the burst properties of ca3 and ca1 neurons. *Neuroscience*, 141:1665–1677, 2006.

[41] Jensen M.S., Azouz R., and Yaari Y. Spike after-depolarization and burst generation in adult rat hippocampal ca1 pyramidal cells. *Journal of Physiology*, 492:199–210, 1996.

[42] Azouz R., Jensen M.S., and Yaari Y. Ionic basis of spike after-depolarization and burst generation in adult rat hippocampal ca1 pyramidal cells. *Journal of Physiology*, 492:211–223, 1996.

[43] Lisman J.E. Bursts as a unit of neural information: making unreliable synapses reliable. *TINS*, 20:38–43, 1997.

[44] Allen C. and Stevens C.F. An evaluation of causes for unreliability of synaptic transmission. *PNAS*, 91:10380–10383, 1994.

[45] Murthy V.N., Sejnowski T.J., and Stevens C.F. Heterogeneous release properties of visualized individual hippocampal synapses. *Neuron*, 18:599–612, 1997.

[46] Miles R. and Wong R.K.S. Excitatory synaptic interactions between ca3 neurons in the guinea-pig hippocampus. *J. Physiol.*, 373:397–418, 1986.

[47] Sayer R.J., Friedlander M.J., and Redman S.J. The time course and amplitude of epsps evoked at synapses between pairs of ca3/ca1 neurons in the hippocampal slice. *J. Neurosci.*, 10:826–836, 1990.

[48] Stevens C.F. and Wang Y. Facilitation and depression at single central synapses. *Neuron*, 14:795–802, 1995.

[49] Creager R., Dunwiddie T., and Lynch G. Paired-pulse and frequency facilitation in the ca1 region of the *in vitro* rat hippocampus. *J. Physiol.*, 299:409–424, 1980.

[50] Zucker R.S. and Regehr W.G. Short-term synaptic plasticity. *Annu. Rev. Physiol.*, 64:355–405, 2002.

[51] Debanne D., Gurineau N.C., Gähwiler B.H., and Thompson S.M. Paired-pulse facilitation and depression at unitary synapses in rat hippocampus: quantal fluctuation affects subsequent release. *J. Physiol.*, 491:163–176, 1996.

[52] Dobrunz L.E., Huang E.P., and Stevens C.F. Very short-term plasticity in hippocampal synapses. *PNAS*, 94:14843–14847, 1997.

[53] Hassoun M.H. *Associative neural memories: theory and implementation*. Oxford University Press, 1993.

[54] Lee A.K. and Wilson M.A. Memory of sequential experience in the hippocampus during slow wave sleep. *Neuron*, 36:1183–1194, 2002.

[55] Dunwiddie T. and Lynch G. Long-term potentiation and depression of synaptic responses in the rat hippocampus: Localization and frequency dependency. *J. Physiol. (Lond.)*, 276:353–367, 1978.

[56] Malenka R.C. and Nicoll R.A. Long-term potentiation - a decade of progress? *Science*, 285:1870–1874, 1999.

[57] Behrens C.J., van den Boom L.P., de Hoz L., Friedman A., and Heinemann U. Induction of sharp wave-ripple complexes *in vitro* and reorganization of hippocampal networks. *Nature Neurosci.*, 8:1560–1567, 2005.

[58] Thomas M.J., Watabe A.M., Moody T.D., Makhinson M., and O'Dell T.J. Postsynaptic complex spike bursting enables the induction of ltp by theta frequency synaptic stimulation. *J. Neurosci.*, 18:7118–7126, 1998.

[59] Lubenov E.V. and Siapas A.G. Decoupling through synchrony in neuronal circuits with propagation delays. *Neuron*, 58:118–131, 2008.

[60] Nadel L. and Moscovitch M. Memory consolidation, retrograde amnesia, and the hippocampal complex. *Curr. Opin. Neurobiol.*, 7:217–227, 1997.

[61] Clark R.E. and Squire L.R. Classical conditioning and brain systems: The role of awareness. *Science*, 280:77–81, 1998.

[62] Bontempi B., Laurent-Demir C., Destrade C., and Jaffard R. Time-dependent reorganization of brain circuitry underlying long-term memory storage. *Nature*, 400:671–675, 1999.

[63] Eichenbaum H. A cortical-hippocampal system for declarative memory. *Nat. Rev. Neurosci.*, 1:41–50, 2000.

[64] Wiltgen B.J., Brown R.A., Talton L.E., and Silva A.J. New circuits for old memories: the role of the neocortex in consolidation. *Neuron*, 44:101–108, 2004.

[65] Wilson M.A. and McNaughton B.L. Dynamics of the hippocampal ensemble code for space. *Science*, 261:1055–1058, 1993.

[66] Siapas A.G.and Lubenov E.V. and Wilson M.A. Prefrontal phase-locking to hippocampal theta oscillations. *Neuron*, 46:141–151, 2005.

[67] Quirk M.C. and Wilson M.A. Interaction between spike waveform classification and temporal sequence detection. *J. Neuroscience Methods*, 94:41–52, 1999.

[68] Schmitzer-Torbert N., Jackson J., Henze D., Harris K., and Redish A.D. Quantitative measures of cluster quality for use in extracellular recordings. *Neuroscience*, 131:1–11, 2005.